Marine Chemistry 268 (2025) 104473

Contents lists available at ScienceDirect

Marine Chemistry

journal homepage: www.elsevier.com/locate/marchem

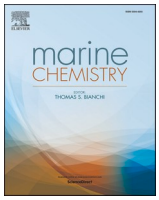

Spatiotemporal variability in benthic-pelagic coupling on the Oregon-Washington shelf

Anna Hughes [*], Clare E. Reimers, Kristen E. Fogaren[1], Yvan Alleau

College of Earth, Ocean, and Atmospheric Sciences, Oregon State University, Corvallis, OR 97331, USA

ARTICLE INFO

Keywords:
Benthic flux
Upwelling
Denitrification
Hypoxia

ABSTRACT

Continental shelf sediments are sinks for dissolved oxygen (DO) and sources of many major and minor nutrients required for oceanic surface primary production resulting in a strong coupling between benthic and pelagic biogeochemical cycling. In this study, we present paired benthic flux and bottom water biogeochemical data collected from two Oregon shelf sites sampled approximately quarter-annually between 2017 and 2019, and from nine other shelf sites, located off central Oregon to southern Washington, and sampled in either July or September 2022. The benthic fluxes were determined using a novel set-up for *ex situ* core incubations. When fluxes were normalized to the respective measured sediment DO flux, ratios aligned well with ratios of past flux estimates from the region which were determined using *in situ* benthic chambers; however, the *ex situ* flux magnitudes are generally lower. Our findings demonstrate sediments acting as net sinks for DO and nitrate, and sources for phosphate, silicate, and ammonium. Shelf-wide estimates of the relative contribution of sediment-remineralized phosphate and silicate to surface waters on the Oregon shelf, indicate that shelf sediments supplied at least 5 ± 7 % and 37 ± 7 % of the available phosphate and silicate during recent summer upwelling seasons, with similar, respective estimates of 2 ± 9 % and 35 ± 11 % during the spring. Remineralization ratios of C:N:P:O_2 corroborate increased denitrification during the summer and weak denitrification during the winter due to a more oxygenated water column in support of previous studies. A multi-tracer water mass analysis also exhibited an increased water-column nitrate deficit during the summer and fall. Benthic denitrification rates, estimated from benthic fluxes, were between 0.2 and 1.8 mmol N m^{-2} day^{-1} and in the range of past assessments during the upwelling season. A simple model, applied to further constrain the contributions to bottom water fixed nitrogen (N) loss under assumptions of benthic boundary layer height and residence time, showed that although sediment denitrification could readily account for total bottom water N losses during the summer, additional water-column denitrification is indicated by the strength of early fall deficits at some stations. Constraining water-column and benthic contributions to fixed N deficits is important for understanding how N-limited primary productivity in this region will respond to projected ocean deoxygenation under anticipated global warming. These results demonstrate the interplay of sediment and water-column remineralization processes across the OR-WA shelf. As in most shallow marine systems, the two are integral to the ecosystem dynamics and responses to environmental change.

1. Introduction

Approximately one third of organic matter produced within continental-shelf environments is exported to the open ocean. This export of organic carbon from continental shelves to the open ocean is estimated to be 0.15–0.35 Pg yr^{-1} and is thought to be a significant driver of CO_2 sequestration within the post-industrial ocean (Bauer et al., 2013; Gattuso et al., 1998; Middelburg et al., 1993; Walsh, 1991). Over 90 % of the organic matter remaining on the shelf is remineralized back into inorganic carbon and nutrients within the water column and sediments of the coastal zone (Bauer et al., 2013; Kelly and Nixon, 1984; Middelburg et al., 1993). In shelf systems, nutrients recycled within the sediments can supply a large proportion of the phytoplankton nutrient demand in the overlying water column, creating a tight relationship between surface-water primary productivity and benthic remineralization (Blackburn and Henriksen, 1983; Cowan et al., 1996; Grenz et al.,

* Corresponding author.
E-mail address: hugheann@oregonstate.edu (A. Hughes).
[1] Present address: *Earth and Environmental Sciences, Boston College, Chestnut Hill, MA, USA*

https://doi.org/10.1016/j.marchem.2024.104473
Received 26 April 2024; Received in revised form 25 October 2024; Accepted 20 November 2024
Available online 26 November 2024

2000; Grenz et al., 2010; Trimmer et al., 1998), which is broadly known as benthic-pelagic coupling (Dale et al., 2017; Ehrnsten et al., 2019; Kopp et al., 2015; Nixon, 1981; Rowe et al., 1975; van de Velde et al., 2023).

Benthic-pelagic coupling may be enhanced within coastal upwelling regions, in comparison to other coastal systems, because of an increased magnitude of local production and subsequent increased rain rate of organic matter available for benthic remineralization (Jahnke, 1996; Thunell et al., 2007; Varela et al., 2004). The Oregon-Washington (OR-WA) continental margin is a highly dynamic, Eastern-Boundary upwelling system located within the northern California Current System (CSS), with variable shoreline geomorphology and offshore bathymetry. The region experiences an extensive range of physical transport and water-column structuring phenomena on temporal scales of days to decades (Adams et al., 2013; Deutsch et al., 2021; Hickey and Banas, 2003; Huyer, 1977; Siedlecki et al., 2015). These phenomena include freshwater delivery from coastal rivers (Goñi et al., 2021), marine heat waves (Wyatt et al., 2022), and intense winter storms (Kniskern et al., 2011), in addition to seasonal upwelling and downwelling cycles (Hickey, 1979; Huyer, 1983; Huyer et al., 1979; Perlin and Moum, 2008).

Coastal upwelling, induced by strong northerly winds, occurs primarily between the months of May and October (Hickey and Banas, 2003; Huyer et al., 1979; Perlin et al., 2005). As the upwelling season progresses, the retention of upwelled waters on the shelf can result in bottom-water oxygen concentrations dropping below the hypoxia threshold of 61 μmol kg^{-1} (1.4 mL L^{-1}) (Chan et al., 2008). With a trend of declining summertime lows in dissolved oxygen (DO) over the past several decades (Bograd et al., 2008; Chan et al., 2008; Chavez et al., 2017), many recent studies have worked to understand the drivers of hypoxia in these bottom waters and how this change may alter carbon sequestration and nutrient cycling in the region (Berelson et al., 2013; Connolly et al., 2010; Fuchsman et al., 2015; Reimers et al., 2016; Siedlecki et al., 2015). Generally, studies conclude that benthic and water-column biogeochemical processes each contribute about 50 % to the autochthonous drawdown of DO within bottom waters during the summer upwelling season on the WA (Connolly et al., 2010), OR (Fuchsman et al., 2015), and Central and Northern CA (Berelson et al., 2013) shelves. However using a ROMS model, Siedlecki et al. (2015) found that bathymetric features affect the retention of shelf waters and that local circulation processes, including circulation-driven divergence, play as important a role as local respiration in creating hypoxic conditions on the shelf. Further, Siedlecki et al. (2015) note key differences between certain Oregon and Washington shelf areas with a larger dominance of respiration on the Oregon shelf due to its greater retentive nature (Barth et al., 2005).

During extended upwelling events, biomass-laden surface waters can be transported offshore, increasing organic matter supply to the outer shelf and slope (Hales et al., 2006). Conversely, upwelling seasons with more intermittent wind reversals and relaxation events have been shown to increase water-mass retention, resulting in a more localized transport of organic matter from surface waters to the mid-shelf region, and heightening DO loss in bottom waters on the shelf (Galán et al., 2020; Segura-Noguera et al., 2023). Under severely low DO conditions, < 24 μmol kg^{-1} (Kalvelage et al., 2011), organic matter in sediments may be primarily remineralized by denitrification, consuming fixed nitrogen (N) in the form of nitrate (Codispoti, 2007; Devol and Christensen, 1993; Fuchsman et al., 2015). The coupling of nitrification-denitrification in the shelf sediments of OR, WA, and CA results in non-Redfield carbon to nitrogen regeneration ratios in sediments (Hartnett and Devol, 2003; Segura-Noguera et al., 2023), and may determine the N loss from bottom waters (Berelson et al., 2013; Devol and Christensen, 1993; Galán et al., 2020). Primary productivity in the region has been determined to be generally nitrogen limited due to excesses of phosphate and silicate over nitrate + nitrite in surface waters and sufficient iron availability stemming from Columbia River and other smaller river inputs, or from shelf and slope sedimentary sources (Chase et al., 2005; Chase et al., 2002; Severmann et al., 2010). Thus, benthic denitrification followed by wind-induced vertical mixing further reinforces a nitrogen-limited system (Fuchsman et al., 2015).

The extent of all avenues of coupling between benthic-pelagic processes is sensitive to environmental factors like wind-forcing, temperature, organic matter input, flow speeds, bottom water dissolved oxygen and nutrient concentrations, the saturation states of minerals, and the presence and activities of benthic fauna that affect benthic remineralization (Aller and Rude, 1988; Alonso-Pérez and Castro, 2014; Caffrey et al., 2010; Ehrnsten et al., 2019). Further once oxygen and nitrate are exhausted, organic matter oxidation can continue through metal reduction and sulfate reduction generating reduced by-products that first accumulate but may be later oxidized when oxygen and nitrate are again available (Reimers et al., 2016).

Biogeochemical models can be helpful in predicting the variability of benthic fluxes as well as the relationships between benthic-pelagic feedbacks and ecosystem functioning (Dale et al., 2017; Ehrnsten et al., 2019; Griffiths et al., 2017). However, accurate depictions and representations of sediment remineralization and benthic-pelagic coupling for model validation are needed (Dale et al., 2017; Kriest and Oschlies, 2008). For the OR-WA margin specifically, Siedlecki et al. (2015) identified the need to improve constraints on spatial variability in the water-column and benthic respiration, and the interannual variability in the source waters upwelled onto the shelf, to improve model prediction capabilities of DO drawdown. Further, coastal systems, including the OR-WA margin, are changing due to global warming and related marine heat waves, emphasizing the need to understand benthic-pelagic feedbacks in these environments to anticipate how they may change under future climate change scenarios (Ehrnsten et al., 2019; Siedlecki et al., 2015).

This study aims to advance the current understanding of benthic nutrient, oxygen, and carbon fluxes on the OR-WA shelf, specifically focusing on the influence of these fluxes on overlying bottom-water chemistry. Property-property relationships of bottom-water solutes and benthic fluxes are examined to investigate organic matter remineralization pathways, and a multi-end member mixing model is applied to assess the contributions of different source waters, water-column remineralization, and other benthic processes to the observed seasonal and spatial variability in DO and nitrate drawdown. To verify estimates of nitrate loss from bottom waters, the NO tracer is applied to bottom water data. A separate mass balance approach is applied to the benthic flux data to estimate N_2 gas fluxes, which serve as a proxy for total benthic fixed nitrogen loss. A simple model is then applied to these independent estimates, to determine the percent contribution of sediment associated fixed nitrogen loss. Additionally, to gauge the relative contributions of nutrients added to the shelf ecosystem through upwelling of offshore waters *versus* those supplied by benthic fluxes, upwelling transport indices are extended to phosphate and silicate and compared to cross-shelf benthic fluxes.

2. Methods

2.1. Site and sampling descriptions

Water-column samples were collected during ten short-duration cruises, conducted onboard the *R/V Oceanus* between 2017 and 2019, along the Newport Hydrographic (NH) line (approximately 44.65°N). During seven of these cruises, incubations of sediment cores were also successfully completed with a new approach described below. Sampling sites along the NH line were designated according to their approximate

depth (in m) and were chosen to represent an inner-shelf (NH30), mid-shelf (NH80), and outer-shelf (NH145) site, respectively.[2]

Water-column and sediment samples were also collected during two short-duration cruises conducted onboard the *R/V Robert G. Sproul* in July and September of 2022. The sites visited during these cruises are broadly referred to as the OW-MS (Oregon-Washington Mid-Shelf) sites and are specifically identified by their closest latitudinal coastal town or their proximity to an area that has been designated for studying Pacific wave energy (Fig. 1). For example, samples collected offshore of Willapa, WA are identified as WLP sites.

For the NH line sites, NH30 and NH80 sediments were both composed primarily of fine sand, while the NH145 site was muddier and exhibited the highest percentages of clay and silt size fractions of all sites. The sites visited on the Washington shelf, located at 46.45°N, were also muddy, largely as a consequence of sediment transport and deposition within the Columbia River littoral cell (McManus, 1972; Nittrouer and Sternberg, 1981). Representative surface sediment properties for all sites are provided in Table 1, and the respective analytical methods are described in section 2.3. The locations, depths and timings of these collections are provided in Tables S1–2 in the supplementary material.

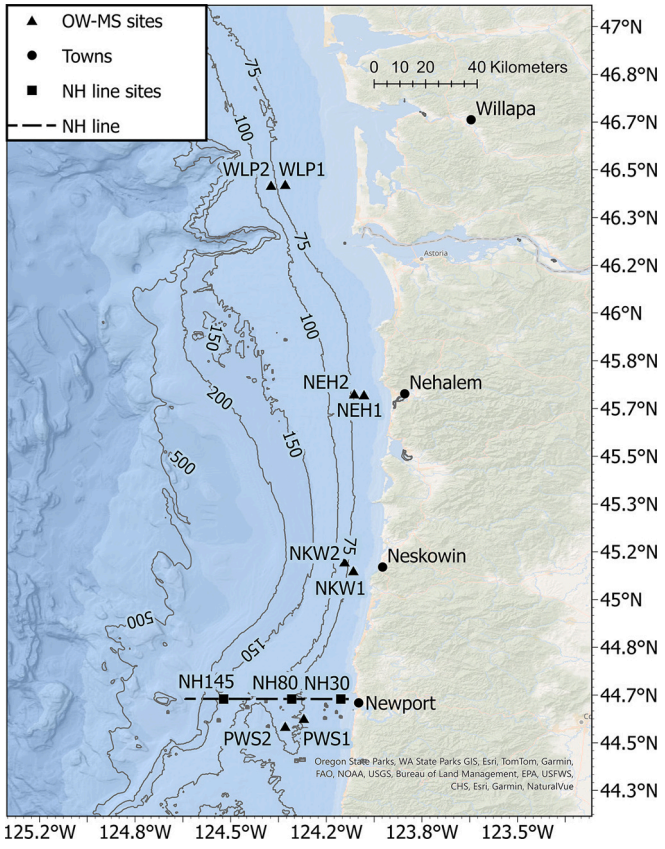

Fig. 1. The full study region, with the Newport Hydrographic (NH) line represented by the black dashed line and black squares denoting the NH30, NH80, and NH145 sites. Black triangles denote the OW-MS sites, which were named by the closest coastal town denoted with black dots, or in one case, a nearby area designated to study Pacific wave energy (PWS1 and PWS2). The contour lines show depth in meters.

[2] Some researchers identify stations along the Newport Hydrographic line by distance from shore in nautical miles. NH80 in this study corresponds to what has been called NH10, because the water depth is 80 m when 10 nm from shore.

2.2. Near-bottom water sampling and processing

CTD-rosette casts were routinely conducted for the collection of bottom waters. The CTD was lowered to within 3–8 m of the seafloor and two or more 10 L Niskin bottles were fired in rapid succession. DO concentrations were determined from sensor measurements (SBE 43) and on chemically-fixed water samples using an amperometric Winkler titration method (Culberson et al., 1991). A comparison between oxygen concentrations obtained from the Winkler method with the oxygen measurements reported by the CTD-mounted SBE 43 sensor, through linear regression analysis, showed good agreement (slope = 1.05 when Winkler on y-axis; R^2 = 0.98) across all cruises and casts (n = 283). Nutrient samples drawn from Niskin bottles were analyzed onshore using standard auto-analyzer colorimetric methods at Oregon State University (Gordon et al., 1993). Dissolved inorganic carbon (DIC) water samples were collected in rinsed 340 mL amber glass bottles, poisoned with 50 μL of mercuric chloride, and analyzed onshore at Oregon State University using a Burke-O-Lator pCO_2-DIC analyzer (Hales et al., 2004), by methods outlined in Evans et al. (2019). Measured DIC and pCO_2 were then used to compute pH and aragonite saturation state using the MATLAB version of CO2SYS (Sharp et al., 2020), with equilibration constants from Millero (2010). Water samples (1 L) for total suspended solids (TSS) and particulate organic carbon/particulate nitrogen (POC/PN), were immediately filtered through pre-combusted (400 °C for 4 h) and weighed, 25 mm, Whatman™ GF/F filters, which were then frozen at sea (−20 °C) for later onshore analysis. In the laboratory, filters were dried at 60 °C for 24 h, reweighed, and then exposed to acid fumes for 24 h to remove inorganic carbon. Dried filters were analyzed using a CarloErba NA-1500 elemental analyzer by the procedure detailed in Goñi et al. (2021) that follows from Verardo et al. (1990).

The CTD sensor data were processed using Sea-Bird SEASOFT software. For all CTD data, *in situ* temperature and salinity were converted to conservative temperature (CT, units of °C) and absolute salinity (SAL, units of g kg^{-1}), and potential density was calculated with input parameters of CT, SAL, and depth (m), using the TEOS-10 subroutines in the MATLAB Gibbs Seawater Package (McDougall and Barker, 2011). Calculated densities were then used to convert volumetric units to units per kilogram of seawater. A total of 269 bottom water samples were considered for further water mass analyses described in section 2.5.

2.3. Sediment core incubation setup, sampling, and processing

Sediment core incubations were performed during the February, May, July, and October 2018, January, April, and July 2019 cruises at NH line sites, and during the July and September 2022 cruises at OW-MS sites, using a unique core incubation method designed around the sediment core collection tube. Details of the method and images of the setup are provided in Hughes (2024) and Fig. S1, respectively. Briefly, sediment cores were collected in acrylic tubes with a radius of 5.3 cm and length of 94 cm using a hydraulically dampened Gravity Corer, designed for recovering sandy sediments (Reimers et al., 2012). Onboard, cores were immediately transported to a cold van where the temperature was pre-set to the approximate *in situ* bottom water temperature. The core's overlying water was siphoned down to ~10 cm above the sediment surface, the minimum determined height for sufficient remaining overlying water volume for sample collection and biogeochemical analyses. A custom-made black Delrin puck (Fig. S2), with two side grooves for X-ring seals, was pushed down to the water interface and remaining air bubbles were carefully removed through an integrated sampling tube that was later used for time-point water collections. Each puck also enclosed a motor for turning a magnet and an attracted stir bar (4 cm by 4 cm) which rotated at 30 rpm at the top of the overlying water column. The slow stirring speed was selected to enable mixing of the overlying water but to prevent sediment resuspension. The optimal speed was identified in preliminary lab experiments. Each resealed core was placed in a temperature-equilibrated, water-filled,

Table 1
Sediment core-top properties determined from individual incubation cores from each study site.

Sampling Date	Site	Interval	Wet Bulk Density (g cm^{-3})	Porosity	Median Grain Size (μm)	% Clay	% Silt	% Sand	%IC	%TC	%TN	% OC
Jul 2018	NH30	0.5-1 cm	1.89	0.32	170	0.4	3.1	96.5	0.02	0.07	0.006	0.05
Jul 2018	NH80	0–0.5 cm	1.59	0.28	276	0.8	2.7	96.5	0.085	0.088	0.008	0.003
Jul 2019	NH145	0–0.5 cm	1.46	0.65	28	11.6	53.5	34.9	1.37	1.42	0.16	0.05
Jul 2022	PWS1	0–0.5 cm	1.49	0.24	240	1.6	4.6	93.9	0.03	0.17	0.021	0.14
Jul 2022	PWS2	0–0.5 cm	1.84	0.33	245	1.6	4.9	93.5	0.04	0.19	0.023	0.15
Sep 2022	NKW1	0-1 cm	1.93	0.38	238	1.9	6.4	91.7	0.04	0.15	0.015	0.11
Sep 2022	NKW2	0–0.5 cm	1.92	0.41	191	2.5	7.0	90.5	0.02	0.17	0.023	0.15
Sep 2022	NEH1	0.5-1 cm	1.87	0.38	212	1.7	3.9	94.5	0.03	0.10	0.008	0.07
Sep 2022	NEH2	0–0.5 cm	1.85	0.44	181	2.7	9.2	88.1	0.08	0.24	0.026	0.16
Sep 2022	WLP1	1–2 cm	1.61	0.61	43	9.7	51.7	38.6	0.09	1.15	0.085	1.06
Sep 2022	WLP2	1–2 cm	1.76	0.51	131	5.1	20.0	74.9	0.29	0.46	0.042	0.17

incubation chamber with a lid to ensure the core remained at bottom water temperature and under low light conditions inside the cold-van. Up to six cores were maintained in incubation simultaneously.

Incubations ran between 24 and 36 h, with periods between time points adjusted to allow for a collection of three to six total time points per core before oxygen saturation dropped below 10 % (about every 4–12 h depending on initial oxygen concentrations and oxygen uptake rates in the cores). For each measurement, the stirring motor of the core was stopped, and a custom device was used to slowly depress the black puck caps against the overlying water, expelling small, carefully measured volumes through the open sampling tube into a 10 mL gas-tight glass syringe with a luer-lock fitting. After flushing the sampling tube, sample water was directed to the flow-through cell of a PreSens Microx T3 micro-fiber optic oxygen sensor *via* a three-way valve at the end of the tubing, and its DO was recorded as percent air-saturation. The luer-lock fitting of the gas-tight glass syringe was attached to the exit side of the flow-through cell to collect timepoint water samples. These samples included 7 mL for shore-based DIC analysis that were transferred to 8 mL borosilicate scintillation vials with poly-ethylene screw caps with poly-seal cone liners, pre-poisoned with 50 μL of mercuric chloride to halt any biological activity. Another 10 mL was stored in a Nalgene™ HDPE bottle, and frozen (−20 °C) for shore-based nutrient analysis. The second sample enabled a repeat oxygen measurement through the flow cell; however, the initial oxygen measurement was used for the flux calculation. After samples were collected, the three-way valve was closed, the oxygen sensor flow cell was disconnected from the sampling tube, and the stirring motor for the core was turned back on for the core to continue to incubate.

Nutrient samples from sediment core incubation experiments were processed unfiltered by the same methods as the CTD-rosette samples detailed in section 2.2. For DIC samples collected during the 2018 and 2019 cruises, samples were analyzed using a UIC Coulometer with a 1 mL sample loop, however, the results were not found to be reliable and therefore these data are not reported. For the DIC samples collected during the 2022 core incubations, samples were processed for DIC with a Finnigan GasBench-II headspace sampler online with a Finnigan DELTAplusXL gas-source isotope-ratio mass spectrometer, with reported precision between 0.5 and 1 %, using a procedure outlined in Torres et al. (2005).

After incubations were completed, sediment cores were extruded at 0.5 cm intervals for sediment depths <1 cm, 1 cm intervals for 1–10 cm, 2 cm intervals for 10–30 cm, and 5 cm intervals for >30 cm, and stored in separate bags at 8 °C. A subset of core samples, including the top 3 cm of incubated cores were processed for grain size, total C and N, and inorganic C. Grain size analyses were carried out using wet sample aliquots introduced into a Bettersizer S6 plus instrument, which detects grain size using laser diffraction. For total C and N analyses, sediment samples were first processed for wet bulk density by weighing known volumes of sediment, samples were then dried at 100 °C for 72 h and reweighed to assess dry bulk density and porosity before being finely ground with a mortar and pestle. Ground samples were transported to the Soil Health Laboratory at Oregon State University, and total C and N contents measured using an Elementar Vario Macro Cube elemental analyzer. The ground samples were also processed for inorganic carbon using a method similar to that used to process the sediment incubation DIC samples. Samples were acidified with concentrated phosphoric acid (85 %) and allowed to react for 12 h before analysis of the evolved CO_2. To capture the evolved CO_2, the septum-sealed sample vials are sampled with a double-needle gas headspace sampler, which flushes the vial with a continuous stream of helium gas from one orifice and samples the headspace, composed of CO_2 and helium gas, with the second orifice. Sediment percent organic carbon values were computed as the difference between percent total carbon and percent inorganic carbon.

2.4. Core incubation calculations and benthic flux derivations

The oxygen concentration of the overlying water at each timepoint of individual core incubations was calculated using oxygen solubility and percent air-saturation measured with the micro-fiber optic sensor. Oxygen solubility was calculated with inputs of sample temperature (obtained during each timepoint sampling), latitude of core collection, and bottom water salinity from the nearest CTD deployment using (http://ocean.ices.dk/Tools/Calculator.aspx). Oxygen, nutrients, and DIC water sample concentration data were then used to calculate fluxes for each component using a linear fit to the time-varying inventory of the solute (in mmol) in the initial overlying water volume of the core, normalized to area. Inventory calculations were made by multiplying measured concentrations times volumes at each time point and adding back amounts contained in water volumes removed during preceding sample collections, over the time of the incubation (Fig. S3). These results were also used to calculate stoichiometric ratios of component fluxes.

Additionally, for each sediment core collected, the measured benthic fluxes of DO, ammonium, and nitrate were applied in a nitrogen and oxygen mass balance, adopted from Fuchsman et al. (2015), to calculate an estimate of the sedimentary flux of N_2 in units of mmol N m^{-2} day^{-1} for each respective core. These benthic N_2 flux estimates serve as a proxy for the total benthic fixed N loss. The calculations assume an elemental stoichiometry from Sarmiento (2006) for the aerobic oxidation of organic matter (Eq. 1) and denitrification (Eq. 2), and assume the relationships between the aerobic carbon oxidation (Ac), carbon oxidized by denitrification (Nc), and production of ammonium (AP) given in Eqs. 3–6.

$$C_{106}H_{175}O_{42}N_{16}P + 150O_2 = 106CO_2 + 16HNO_3 + H_3PO_4 + 78H_2O \quad (1)$$

$$C_{106}H_{175}O_{42}N_{16}P + 94.4HNO_3 = 106CO_2 + H_3PO_4 + 109.2H_2O + 47.2N_2 + 16\,NH_3 \quad (2)$$

$$AP = (16/106)Ac + (16/106)Nc \quad (3)$$

$$DO_{Flux} = (150/106)Ac + 2\left(AP + NH^{+}_{4,Flux}\right) \quad (4)$$

$$NO^{-}_{3,Flux} = (94.4/106)Nc - AP - NH^{+}_{4,Flux} \quad (5)$$

$$N_2 = (47.2/106)\mathrm{Nc} = (7.7/150)\left(DO_{Flux} + 150\Big/16\left(\mathrm{NH}^{+}_{4,\mathrm{Flux}} + 114.5\Big/94.4NO^{-}_{3,Flux}\right)\right) \quad (6)$$

2.5. Water mass analysis

An optimum multiparameter analysis (OMPA) was conducted utilizing the bottom water CTD/Niskin bottle data to distill chemical component contributions from water-column mixing *versus* water-column remineralization processes or any other unaccounted-for process. OMPA was initially developed by Johannes Karstensen and Matthias Tomczak (Tomczak, 1981). The OMPA method assumes that water masses can be represented as proportional combinations of source water types, with these types representing theoretical water-mass endmembers or an average of observed water masses with defined properties such as temperature, salinity, oxygen, phosphate, and nitrate (Tomczak, 1999). Water property data from a location can then be decomposed into a linear combination of these source water types through inverse modeling, enabling the assessment of water-mass contributions and variation in these contributions over time in a specific region (Tomczak, 1981). Classical OMPA assumes that water-mass properties are conservative within a data set; however, oxygen, nitrate, and phosphate are at best semi-conservative, as these species are products or reactants in many biogeochemical processes.

For this study, the Python package "*pyompa*" was used to conduct the analysis, which includes several improvements upon the original "classical" OMPA method, applying what is known as "extended OMPA" or eOMPA, which adds a hard constraint on mass conservation and an extension to allow for remineralization within the water masses along their advective pathway (Shrikumar et al., 2022). The *pyompa* package was applied using Google Colab, through a user-friendly script developed and personally distributed by Dr. Natalya Evans (University of Santa Barbara). Details on the system of equations, theory, calculations, and normalization of the eOMPA method and its implementation in *pyompa* are provided in the pyompa technical note (Shrikumar et al., 2022).

The chosen input parameters used for this study's eOMPA analyses were CT, SAL, DO, nitrate, phosphate, and silicate due to their well-characterized nature in the dataset and the water types of the region. The weightings for these parameters were determined by considering both the measurement uncertainty and the uncertainty present in the values determined for the water types resulting in the weighting of 10:10:1:1:1:1 for CT:SAL:DO:nitrate:phosphate:silicate, respectively. An analysis of the choice of weightings was conducted in Hughes (2024), however, different weightings did not significantly alter the results of the model.

Another crucial component of eOMPA is correctly identifying the end member water types in the region of study. With this study being centered in a shelf environment, the selection of the water types involved balancing two criteria: that the water types characterized the seasonal variability and that the end members were defined close to the region of study to maximize the model's ability to capture smaller, local signals, both within the water column and potentially associated with benthic fluxes. To characterize the water-type endmembers, CTD and bottle data, collected during the 37 cruises of the CCS Long-term Observation Program (LTOP) from 1997 to 2004 as part of the U.S GLOBEC program (NEP project), were used (Fleischbein, 2001). This dataset was selected due to its large spatiotemporal coverage and its inclusion of temperature, salinity, DO, nitrate, phosphate, and silicate data.

Generally speaking, there are two primary currents controlling the distribution of near-bottom water masses along the Oregon continental shelf, the California Undercurrent, identified here as NHCUC, which transports relatively salty equatorial water northward along the U.S. west coast, and the California Current, identified here as NHSUB, which is responsible for transporting relatively fresh subarctic water southward from the Gulf of Alaska (Barth and Wheeler, 2005; Hickey and Banas, 2003; Huyer, 1977; Huyer et al., 2007; Landry et al., 1989). Additionally, during the spring and summer months, cold, salty water is upwelled onto the shelf as a result of strong northerly winds. The upwelled water mass, with its core located between 80 and 100 m (Barth et al., 2005; Barth and Wheeler, 2005), is defined as NHSUP. Along the Oregon Coast during winter, a northward-flowing coastal current arising from buoyancy forcing and transport driven by the Davidson current also determine water properties (Mazzini et al., 2014), which are identified here by a winter water type, NHWS. Specific details for how water types were characterized are provided in Hughes (2024). Parameters for the water types are presented in Table 2, and T-S plots with the water types are shown in the supplementary material (Fig. S4). Additionally, to account for aerobic remineralization within the water types along their advective path, a stoichiometric "Redfield ratio", taken here as −150:16:16:1 for DO to nitrate to silicate to phosphate (Anderson and Sarmiento, 1994; Sarmiento, 2006), was applied in the analysis.

2.6. Bottom water nitrogen loss estimates using the NO tracer

In addition to the eOMPA, the magnitude, seasonality, and significance of bottom water nitrate loss was also assessed using a similar, but separate approach from Segura-Noguera et al. (2023). Bottom water fixed N loss was calculated using an NO tracer (Eq. 7), adjusted from the NO tracer given in Broecker (1974) by further correcting the bottom water DO concentration to account for the DO consumed during oxidation reactions (Eq. 8). The NO tracer was initially developed as a conservative water-mass tracer (Broecker, 1974), with the coefficient for the nitrate concentration chosen such that the nitrate added to the water column by aerobic remineralization is just balanced by the DO consumed. Here, we use the NO tracer to track fixed N loss in bottom waters. DIN denotes the sum of inorganic nitrogen species in seawater (Eq. 9). ΔDO:ΔN represents the change in DO with respect to the change in nitrate *via* Redfield remineralization, taken here from Sarmiento (2006) as −150:16 (Eq. 1). Under strict, Redfield-only remineralization, the tracer should remain constant, however, changes in this tracer represent N loss from other processes such as water-column and sediment denitrification when bottom water DO is low (Bianchi et al., 2018; Canfield, 1994; Segura-Noguera et al., 2023). NO_{ref} represents the NO value of the source waters, which here is calculated for each CTD sample point, using the nitrate and DO concentration outputs from the eOMPA water mass analysis as the expected concentration (DIN_{exp} and $DO_{exp,corr}$, respectively) (Eq. 10). Positive N loss values represent any N loss from denitrification in either the water column or sediment during the bottom water's residence time on the shelf (Eq. 11).

$$NO = DO_{corr} + (\Delta DO : \Delta N)^{*}(DIN) \quad (7)$$

Table 2
Water types determined for the Oregon-Washington shelf, as described in section 2.5, which were used for the eOMPA model. NHSUP represents the summer upwelled water type, NHSUB represents the subarctic water type in the California Current, NHWS is the winter water type representing the mid-shelf Coastal Current, and NHCUC is the California Undercurrent water type.

Water type	CT (°C)	SAL (g kg^{-1})	PO_4^{3-} (μmol kg^{-1})	NO_3^- (μmol kg^{-1})	Si (μmol kg^{-1})	DO (μmol kg^{-1})	σ_θ (kg m^{-3})
NHSUP	7.6	33.9	2.32	29.4	47.2	95.5	26.6
NHSUB	9.8	33.5	1.91	19.6	25.2	112.5	26.0
NHWS	12.4	32.7	0.75	3.8	6.4	265.2	24.9
NHCUC	8.4	34.0	2.27	28.1	34.2	158.0	26.6

$$DO_{corr} = [DO] - 0.5*\left(\left[NO_2^-\right]\right) - 2*\left(\left[NH_4^+\right]\right) \quad (8)$$

$$DIN = \left[NO_3^-\right] + \left[NO_2^-\right] + \left[NH_4^+\right] \quad (9)$$

$$NO_{ref} = DO_{exp,corr} + (\Delta DO : \Delta N)*\left(DIN_{exp}\right) \quad (10)$$

$$N_{loss} = \left(NO_{ref} - NO\right)/(\Delta DO : \Delta N) \quad (11)$$

To assess benthic and water-column contributions to the observed bottom water N deficit, the system was additionally constrained with Eq. 12

$$\%Benthic\ N = \frac{N_2 * \frac{\tau}{BBL_{height}}}{N_{loss}} * 100 \quad (12)$$

where benthic N_2 flux determinations (N_2), calculated from measured benthic flux data as described in section 2.4, were multiplied by an estimate of the bottom water residence time (τ, in days) and then divided by a realistic benthic boundary layer (BBL) height (in m) to assess the benthic N sink in units comparable to the total bottom water N loss (N_{loss}). By this approach, we assumed BBL heights from 5 to 15 m (Barth et al., 2005; Kurapov et al., 2005-09-01; Perlin et al., 2005), and residence times of 7–21 days (Adams et al., 2013; Fuchsman et al., 2015) to evaluate the system. This simple model was only applied to the upwelling season data from NH80 and the OW-MS sites.

2.7. Upwelling transport and nutrient indices and calculations of comparative benthic source contributions

To assess vertical upwelling rates during cruises, daily-averaged transport indices between 43 and 46°N were obtained for days between December 2017 and September 2022 (Fig. S5). These measures are quantified from observational data and regional models and reported by latitude and day through the Coastal Upwelling Transport Index (CUTI) and the Biologically Effective Upwelling Transport Index (BEUTI), with records beginning in 1988 (https://mjacox.com/upwelling-indices/; (Jacox et al., 2018). CUTI values represent a measure of the vertical transport near the coast and are reported in units of volume of vertical transport per second per meter of coastline ($m^2\ s^{-1}$), while BEUTI values (calculated as the product of estimated CUTI values and the respective measured nitrate concentration at the base of the mixed layer) represent an estimate of the transport flux of nitrate into the mixed layer from waters originating off the shelf and are given in units of mmol $m^{-1}\ s^{-1}$ (Jacox et al., 2018).

Monthly averaged BEUTI indices from 45°N were further averaged seasonally for the spring and summer of 2018–2022, then multiplied by the ratios of phosphate to nitrate, and silicate to nitrate concentrations of the upwelled source water type we identified as NHSUP (Table 2). These computations were assumed to serve as a measure of the average, seasonal vertical transport rate of phosphate and silicate associated with cross-shelf upwelling (units of mmol $m^{-1}\ s^{-1}$).

Comparative shelf-wide benthic fluxes were estimated using the measured phosphate and silicate benthic fluxes from this study. Measured fluxes of phosphate and silicate were averaged by site for the spring and summer, and then multiplied by the approximate shelf width represented by each site. These widths were estimated from where the NH line crosses depth contours (Fig. 1) and determined to be 7.0 km, 10.9 km and 20.7 km for NH30 (0–50 m), NH80 (50–80 m), and NH145 (80–150 m), respectively. These depth-range estimates were summed together, to represent the full-shelf benthic contribution, then were adjusted to be the same units as BEUTI values to enable comparison, and finally, divided by the sum of the respective BEUTI value and benthic flux value to provide an estimated range of the percent contribution for phosphate and silicate to the cross-shelf water column. Flux data from NH145 was only available from the summer and to overcome this limitation, the same ranges of measured summer phosphate and silicate fluxes at NH145 were assumed for the spring, as flux ranges for the inner and mid-shelf appeared similar across these two seasons. Nitrate and DO were excluded from this analysis as these species are predominately consumed by OR-WA shelf sediments, and other mass balance techniques, described above, were applied to estimate how these benthic processes impact the water column.

3. Results

3.1. Benthic fluxes and benthic flux remineralization ratios along on the OR-WA shelf

The measured benthic fluxes of DO, phosphate, nitrate, and DIC determined in this study are plotted pairwise to illustrate magnitudes and demonstrate how the remineralization exchange ratios varied spatially and seasonally, with each point representing a unique core incubation (Fig. 2). The expected stoichiometric ratios of aerobic organic matter remineralization (Redfield ratio), taken here from Sarmiento (2006) to be −150:106:16:1 for DO to inorganic carbon to nitrate to phosphate (Eq. 1) are represented in Fig. 2, by the solid bold lines and adjacent respective ratio values. The expected stoichiometric ratios for denitrification, taken from Paulmier et al. (2009), *i.e.*, −94.4:106:1 for nitrate to inorganic carbon to phosphate (Eq. 2), are displayed as dashed lines with adjacent, respective ratios in Fig. 2. Intermediate dotted lines and adjacent ratio values depict the expected stoichiometric ratios that would result from a 1:1 or 50 % contribution of both aerobic Redfield remineralization and denitrification. Averaged benthic fluxes for all parameters, including silicate, ammonium, and nitrite, are provided in the supplementary material and are grouped by the season of collection[3] and site (Table S3).

Overall, sediments acted as a year-round sink for DO (Fig. 2B, E, F), a general sink for nitrate (Fig. 2A, C, E), and a general source for ammonium (Table S3 and Fig. S6), phosphate (Fig. 2C, D, F) and silicate (Table S3 and Fig. S6). However, incubation fluxes also exhibited both seasonal and spatial variability (Fig. 2 and Fig. S6). Focusing on the NH80 site which had the greatest seasonal coverage, average DO fluxes were at a minimum during the spring and summer (−1.4 mmol $m^{-2}\ day^{-1}$) and reached a maximum during the winter (−2.0 mmol $m^{-2}\ day^{-1}$), while nitrate fluxes were near zero and positive during the winter (0.01 mmol $m^{-2}\ day^{-1}$) and consistently negative during the spring, summer, and fall (−0.3 mmol $m^{-2}\ day^{-1}$). NH80 silicate fluxes increased through the annual winter-fall progression (Fig. S6 and Table S3).

DO fluxes at the NH30 site showed higher rates during the spring compared with summer collections. Further, NH30 DO fluxes were nearly double those found at NH80 (average spring uptake of −3.1 mmol $m^{-2}\ day^{-1}$). (Unfortunately, no winter or fall incubation fluxes were collected at NH30 due to coring challenges under high sea states and limited ship time.) NH30 nitrate fluxes too showed an increase in magnitude compared to those observed at NH80, with an average summer uptake of −0.41 mmol $m^{-2}\ day^{-1}$. Phosphate fluxes were close to zero or into the sediment at both sites in the spring but generally out of the sediment in the fall and winter, while ammonium fluxes were primarily out of the sediment at NH30 and NH80. Outliers were present in the phosphate and ammonium fluxes measured from three NH30 cores, two during May of 2018 and one during April of 2019, due to the presence and perishing of multiple sand dollars (*Dendraster excentricus*), small hermit crabs (Paguroidea), and other invertebrates at the surface of these cores during their incubations. All flux data for these cores were removed from subsequent analyses and are not presented in Fig. 2 or Table S3.

[3] In this study, winter is considered the months of December, January, and February; spring is March, April, and May; summer is June, July, and August; and fall corresponds to September, October, and November.

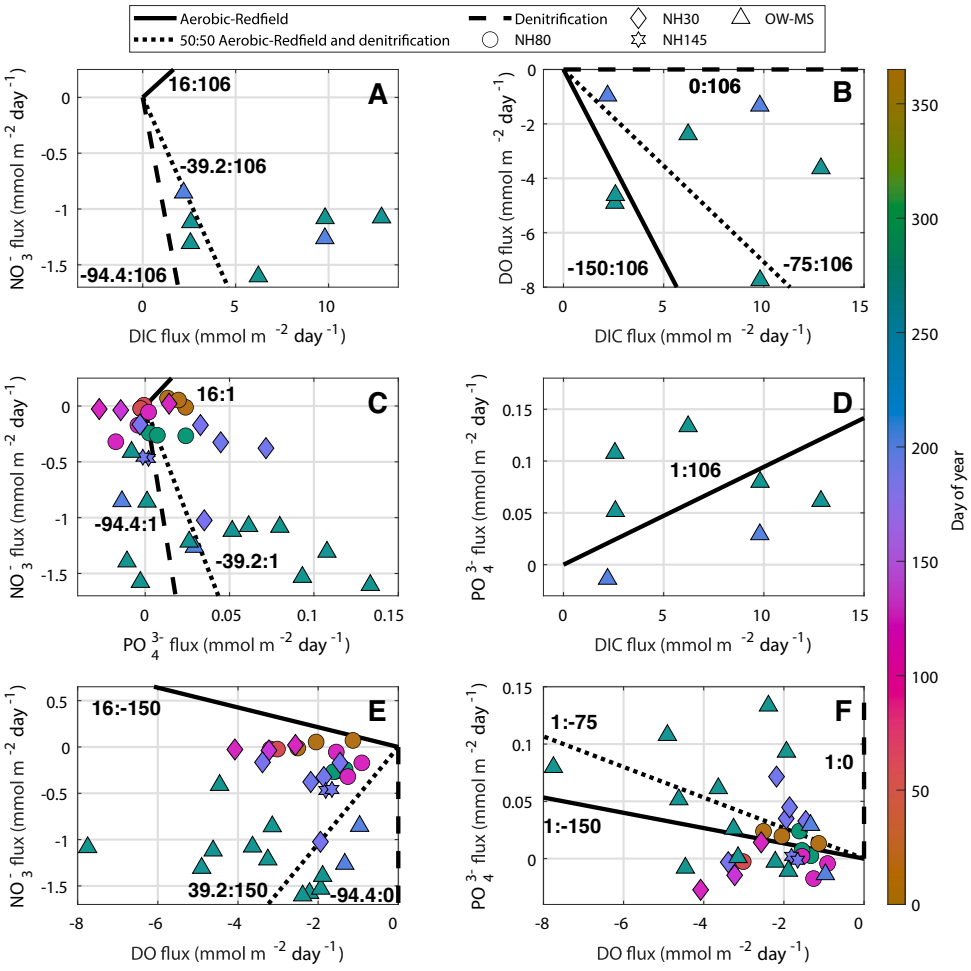

Fig. 2. Pairwise plots of DO, DIC, NO_3^-, and PO_4^{3-} benthic fluxes from individual core incubations. The shape color indicates the day of year of the collections for NH30 (dots), NH80 (diamonds), and OW-MS sites (triangles). The lines show the expected ratio in a system with only aerobic remineralization (bold) (Eq. 1), with a 50 % contribution from aerobic remineralization and denitrification (dotted), and with only denitrification (dashed) (Eq. 2), with the respective ratios for these relationships provided adjacent to the lines.

Benthic fluxes showed high spatial variability between the four mid-shelf areas, the OW-MS sites, visited during July or September of 2022 (Fig. 2 and Table S3), with sediments acting as sinks for DO and nitrate and sources for silicate, ammonium, phosphate, and DIC. Fluxes of DO, nitrate, and silicate showed greater magnitudes at these sites compared with the NH line, with silicate fluxes ranging between 3.2 and 10.4 mmol m^{-2} day^{-1} compared with the average fall flux of 1.49 mmol m^{-2} day^{-1} at the NH80 site. Phosphate fluxes at these sites were also greater than those observed along the NH line with an average value of 0.049 compared to 0.011 mmol m^{-2} day^{-1} observed at the NH80 site. The cores with the highest observed nitrate uptake fluxes were from two sites on the Washington shelf (WLP1 & 2) and also exhibited the highest observed ammonium and nitrite effluxes. These two sites had severely hypoxic bottom waters and consequentially showed the lowest DO uptake flux of all sites visited during September 2022. The two sites off the Washington shelf also exhibited different sediment composition and core top characteristics than the Oregon mid-shelf sites, particularly their significantly higher percentages of silt, clay, and total carbon and nitrogen (Table 1).

With respect to benthic flux ratios, both NH30 and NH80 exhibited seasonal signatures (Fig. 2C, E, and F). For the flux ratios of nitrate to DO and nitrate to phosphate, winter ratios congregated close to the aerobic Redfield ratio, while summer and fall ratios were closer to ratios expected for remineralization by combined aerobic oxidation of OM and denitrification. For nitrate to phosphate and phosphate to DO ratios, some values fell outside of expected ranges, specifically when phosphate fluxes were into the sediment (Figs. 2C and F).

In the OW-MS data, there were higher magnitude fluxes and greater variability in ratios than observed at the NH80 and NH30 sites (Fig. 2C, E, and F). In addition to ratios of DO, nitrate, and phosphate, the OW-MS data also includes ratios to DIC fluxes, which similarly showed a wide range of variability (Fig. 2A, B, and D). For nitrate to DIC and nitrate to DO, we observe ratios between the aerobic Redfield and denitrification only stoichiometric ratios, while for DO to DIC and phosphate to DO we observe values from above the expected ratio for aerobic Redfield remineralization to that of denitrification only (Fig. 2A, E and B, F, respectively). Focusing on the DO to DIC ratios, although most also fell between the aerobic-Redfield and denitrification-only expected ratios (Fig. 2B), two ratios fell just outside the expected aerobic-Redfield ratio. These two ratios came from sites NKW1 and NKW2 which exhibited relatively high bottom water DO (> 95 μmol kg^{-1}) compared with the other OW-MS sites, resulting in some of the highest observed core incubation DO fluxes of −4.9 and − 4.6 (mmol m^{-2} day^{-1}) that may have reflected transient oxidation of accumulated inorganic reductants. Additionally, ratios of nitrate to phosphate fluxes exhibited some values outside that expected for denitrification-only remineralization, indicating the presence of other diagenetic reactions taking up phosphate (Fig. 2C).

Measured benthic fluxes of DO, ammonium, and nitrate were also used in a nitrogen and oxygen mass balance approach detailed in section

2.4, to estimate benthic N_2 fluxes, which were not measured during the sediment core incubations. The N_2 flux estimates at NH80 were found to reach a maximum during the summer, in comparison to the spring data (Table 3). N_2 flux estimates were greatest at the OW-MS sites in the late summer and early fall, ranging between 1.1 and 1.8 mmol N m^{-2} day^{-1}, and were higher than the maximum observed at NH80 during summer collections, despite the similar depths of these sites (Table 3).

3.2. Bottom water data

Bottom-water solute concentrations showed seasonality across the NH line with all DO, phosphate, DIC, and nitrate measurements presented in Fig. 3. These and all other bottom water concentrations, pH, aragonite saturation state, and POC determinations are reported as average values by season (regardless of year) and site in the supplementary material (Table S4). Average DO concentrations were lowest within the summer samples (NH80: 55 μmol kg^{-1}, NH30: 83 μmol kg^{-1}) and highest in winter collections (NH80: 216 μmol kg^{-1}, NH30: 253 μmol kg^{-1}) when the water column was often well mixed (Reimers and Fogaren, 2021). Conversely, bottom-water nitrate, phosphate, silicate, and DIC concentrations were greatest in the summer and fall collections and reached a minimum during the winter (Fig. 3). Bottom-water pH followed a similar pattern to bottom-water DO, with its lowest values observed during July (NH80: 7.6, NH30: 7.6) and maximum values during January (NH80: 7.9, NH30: 8.0).

The bottom water concentration data from the July and September 2022 cruises along the OW-MS sites aligned with NH line bottom-water summer and fall patterns, with low DO concentrations and high nitrate, phosphate, DIC, and silicate concentrations (Fig. 3, Table S4). The lowest bottom-water pH values were recorded during the September cruise which visited the OW-MS sites, with nearly all bottom water aragonite saturation state estimates falling below a value of 1 (Table S4). POC concentrations were markedly greater within the shallow bottom waters of NH30 than at any other site in spring, summer and fall samples, averaging 0.3–0.4 mg L^{-1} (Table S4).

The respective ratios (or slopes) of property-property plots of bottom-water DO, DIC, and nutrients show Redfield-like values, indicative of the aerobic remineralization of marine organic matter that dominates in the water column and in surface sediments, especially in the winter. When slopes were derived with season-specific data, winter values (nitrate to phosphate = 15.0, DO to nitrate = −6.5, and DO to DIC = −0.75) generally fall closer to the aerobic Redfield-like values of nitrate to phosphate = 16, DO to nitrate = −9.4, and DO to DIC = −1.4, than summer slope ratios (nitrate to phosphate = 16.8, DO to nitrate = −4.6, and DO to DIC = −0.64).

3.3. Water-mass analysis and bottom water N loss

To assess the contributions of different regional water types, mixing and remineralization to bottom water DO, nitrate, phosphate, and silicate concentrations, an eOMPA water-mass analysis was applied and indicated both strong seasonality in the water types present on the shelf and some cross-shelf variability between the NH30 and NH80 sites (Fig. S7). During the winter months, particularly January and February, a well-mixed water column was confirmed, with similar combinations of NHCUC, NHWS and NHSUB water types present across the NH30 and NH80 sites in January 2018 and January 2019, and NH80 in February 2018. Summer and early fall bottom waters were dominated by upwelled NHSUP water except for some NH30 and NH80 samples in July 2019 where the NHSUB (subarctic water mass) dominated. The spring, late fall, and early winter collections show more variable water-mass compositions (even within a tidal cycle), indicative of the transitional periods between upwelling and downwelling regimes on the OR-WA shelf. Evidence of these transitions was also apparent in the CUTI data, which are presented for each cruise month in Fig. S5.

Residuals output by the eOMPA analysis for DO, nitrate, phosphate, and silicate are shown in Fig. 4 and interpreted as additional sources or sinks that were unaccounted for by the model. For DO and nitrate, most residuals are positive, indicating an additional, unaccounted-for sink for DO and nitrate. For DO, this sink appears largest during the spring, while for nitrate this sink appears largest and quite strong in the late summer and fall. For phosphate and silicate, there appears to be more variability in the direction of the residuals, with an additional phosphate sink more consistently in the winter and spring and source during the summer, and an unaccounted-for source of silicate influencing the bottom water in summer and early fall.

N loss values estimated using the NO tracer method (Eqs. 7–11) from the bottom water data and averaged by site and season, are listed in Table 3 (fourth column). N loss estimates were similar in magnitude and seasonality to the eOMPA residuals shown in Fig. 4B which were also averaged and listed for comparison in Table 3. N loss estimates at NH80 appeared to increase from spring to summer, while N loss values for the OW-MS sites were greater, aligning closely with the trend noted in the eOMPA nitrate residuals.

To further investigate the processes contributing to the observed bottom water N deficit, the system was additionally constrained with Eq. 12. The resulting %Benthic N uptake ranges are presented in Table 3, and are quite broad, a caveat of the large input ranges of BBL heights and residence times as these parameters were not measured in this study. The lowest range was observed in the early fall OW-MS data, with the % Benthic N uptake found to range from 13 to 117 %, while the largest range was observed in the NH80 spring data (47–420 %). The summer % Benthic N ranges from both NH80 and OW-MS fell in between these extremes and were very similar in magnitude (Table 3).

Table 3
Seasonally averaged N_2 fluxes, N loss estimates, and NO_3^- residuals from the approaches applied in this study. Using Eq. 12 and assuming residence times from 7 to 21 days and BBL heights of 5–15 m, these determinations were used to compute ranges for the %Benthic N uptake.

Site	Season	N_2 (mmol m^{-2} day^{-1})	N loss (μM)	NO_3^- residuals (μM)	%Benthic N uptake
OW-MS	Summer	1.3	3.8	4.0	15–144
OW-MS	Fall	1.7	6.1	6.7	13–117
NH80	Spring	0.4	0.4	0.4	47–420
NH80	Summer	0.5	1.4	1.4	17–151

3.4. Benthic contribution to upwelled water nutrient supply

Measured sediment incubation nutrient fluxes, extrapolated across the shelf at the NH line, were compared with coinciding BEUTI upwelling indices to quantify the relative importance of these processes for fueling surface water primary productivity during the upwelling season (Table 4). For this region of the shelf, the average percent contributions of phosphate and silicate to the overlying water from sediment regeneration as represented by the NH line sediment incubations during the summer were 5 ± 7 % for phosphate and 37 ± 7 % for silicate. During the spring, these estimates were similar, with the phosphate contribution estimated to be 2 ± 9 % and the silicate contribution estimated to be 35 ± 11 %. Upwelled contributions of phosphate and silicate in the summer were over twice as large as those in the spring at 45°N (Table 4). For benthic fluxes, inner shelf contributions of phosphate and silicate were also significantly lower in the spring compared with summer contributions, while mid-shelf phosphate and silicate contributions were greater, although more variable, in the spring compared with summer values. The outer shelf showed a low contribution of phosphate in the summer, but a high contribution of silicate, in comparison to the inner and mid-shelf.

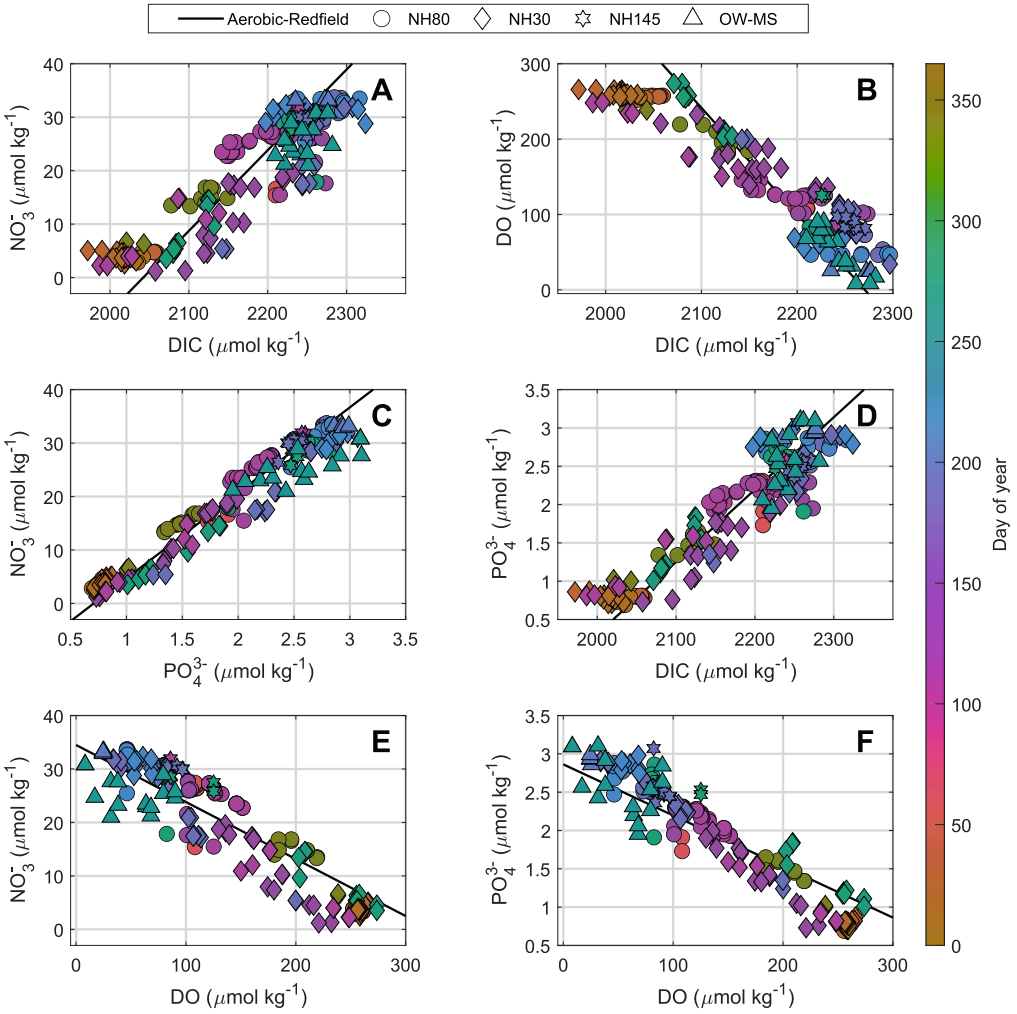

Fig. 3. Pairwise plots of all bottom water concentration data for DO, DIC, NO_3^-, and PO_4^{3-} for NH30 (diamonds), NH80 (circles), and OW-MS sites (triangles). The black line in each plot represents the expected exchange ratio from Aerobic-Redfield like remineralization (Eq. 1) and is centered at the average respective concentration values.

4. Discussion

4.1. Comparison of benthic flux data to past studies on the OR-WA shelf

Although *ex situ* incubations are the most common method for measuring benthic fluxes (Jørgensen et al., 2022), shipboard or laboratory incubations of cores from coastal environments tend to yield benthic fluxes that are smaller in magnitude than *in situ* benthic chambers, with most comparisons focusing on total oxygen uptake (TOU) (Archer and Devol, 1992; Glud et al., 2003; Glud et al., 1998). *Ex situ* DO flux measurements are often 2–3 times lower than *in situ* because core incubations struggle to accurately represent *in situ* benthic faunal abundance and activity (Glud and Blackburn, 2002; Glud, 2008; Glud et al., 2003; Jørgensen et al., 2022). Glud et al. (1994) also found that TOU rates measured using benthic chamber incubations were between 1.2 and 4.2 times greater than diffusive oxygen uptake (DOU) fluxes, derived from *in situ* DO microprofiles, and that this difference correlated with the abundance of macrofauna in the sediment.

Methods that remove or separate the sediment from the natural environment are additionally known to exclude many forms of physical advection that may enhance benthic exchange (Aller, 2014; Jørgensen et al., 2022). For benthic oxygen fluxes, the eddy correlation method is an alternative, noninvasive method that relies on measurements of velocity and DO with sensors usually positioned 15–30 cm above the sediment-water interface. Fluxes derived using eddy covariance methods represent exchanges under natural flow over 10s–100s m^2 of seafloor, and they are especially useful for studying permeable sediments influenced by strong currents and wave motions (Berg et al., 2003; Berg et al., 2022; Berg et al., 2007). Reimers et al. (2012) did compare oxygen fluxes measured with eddy covariance to those measured with *in situ* benthic chambers on the Oregon shelf in summer and surprisingly found chamber O_2 consumption rates exceeded the EC fluxes by factors of 1.2–1.8. This was speculated to reflect either enclosure effects, the different spatial and temporal scales of the measurements, and/or inhomogeneous benthic respiration rates. These methodological and spatial factors are important to consider here as well, where additional solutes affected by benthic respiration reactions are the focus.

To provide a comparison to previous benthic flux studies, ratios were computed for each set of incubation measurements relative to the respective measured DO flux for that incubation and plotted against water depth (Fig. 5). Included were past studies that employed *in situ* benthic chambers (Berelson et al., 2013; Fuchsman et al., 2015; Hartnett and Devol, 2003) (Table S5). These past studies generally reported larger flux magnitudes than were determined with the core incubations of this study. As was discussed above, chambers will capture some of the *in situ* processes such as fauna respiration and bio-irrigation that contribute to fluxes of solutes, while the *ex situ* incubations are mostly

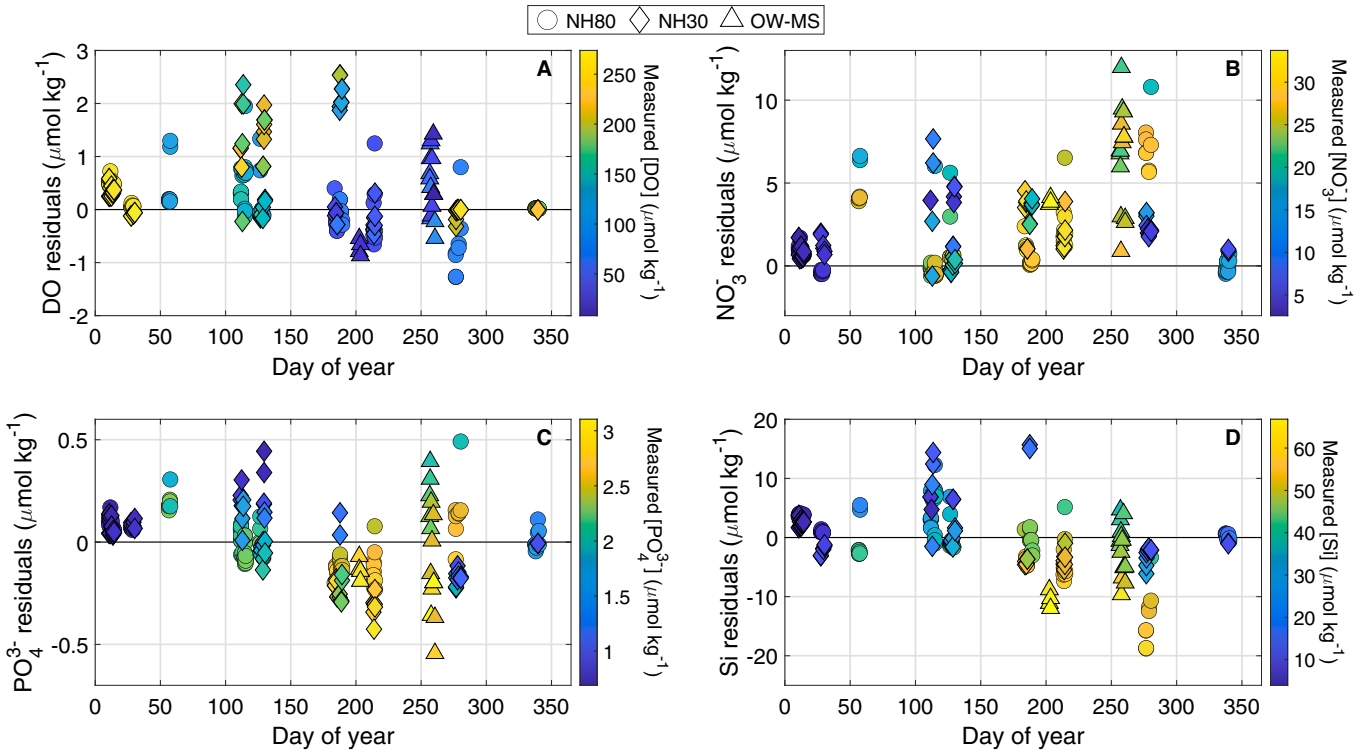

Fig. 4. Residual concentrations of DO (A), NO_3^- (B), PO_4^{3-} (C), and Si (D), computed as the difference between the expected concentration from the eOMPA water mass analysis (see section 3.3) and the respective measured concentration, plotted by the sampling day of year on the horizontal axis. The shape color represents the respective measured concentration for each constituent.

Table 4
Spring and summer, seasonally-averaged total upwelled phosphate and silicate contributions, and seasonal averages of the benthic flux contributions for shelf regions represented by NH30, NH80, and NH145, which were used to calculate overall estimates of the average percent contributions of the benthic fluxes of phosphate and silicate to surface water nutrient concentrations during these seasons, respectively.

Nutrient	Calculated upwelled contribution (mmol m^{-1} s^{-1})	Inner shelf flux contribution (mmol m^{-1} s^{-1})	Mid-shelf flux contribution (mmol m^{-1} s^{-1})	Outer shelf flux contribution (mmol m^{-1} s^{-1})	Mean Overall Benthic Contribution (%)	SD
Spring						
Phosphate	0.081	−0.0007	0.0022	0.0001*	2 %	9 %
Silicate	1.64	0.067	0.126	0.695*	35 %	11 %
Summer						
Phosphate	0.191	0.003	0.001	0.0001	5 %	7 %
Silicate	3.88	0.113	0.168	0.695	37 %	7 %

* Due to a lack of spring flux data from NH145, flux estimates were assumed to be the same as the summer values.

limited to capturing the diffusive flux of solutes across a relatively small surface area of a core (Aller and Aller, 1998; Archer and Devol, 1992; Glud et al., 2003; Jørgensen et al., 2022). Normalizing the fluxes for each benthic chamber and sediment core incubation to the respective measured DO flux for that incubation, enabled the relative comparison of the *ex situ* sediment incubation flux estimates made here with past *in situ* benthic chamber flux estimates, both for how fluxes varied seasonally, spatially, and with depth, and for their effects on bottom water nonconservative properties, *e.g.*, nutrient ratios.

Flux ratios for nitrate, phosphate, ammonium, silicate, and nitrite to DO compared similarly to those of past studies, especially when accounting for seasonal variation (Fig. 5 and Table S5). For nitrate to DO fluxes, within the depth range of 40 to 150 m, ratios generally fell between 0.05 and 0.35 (since both solutes exhibited negative fluxes), with four higher values found in the OW-MS results (Fig. 5A). Regarding the high ratios that fell out of the range observed in Fuchsman et al. (2015), measured DO fluxes were lower in magnitude and measured nitrate fluxes were nearly double from the PWS1&2 sites compared with other summer data previously observed, despite being at similar depths. The other two points are from the Washington margin (WLP1 & 2) and exhibited the greatest nitrate uptake rates of all measured flux data (Fig. 2E), a likely result of enhanced sediment denitrification due to the hypoxic waters present at these sites. The average winter ratio from NH80 was the lowest and only negative ratio, a result of the average positive nitrate flux observed during the NH80 winter cruises (Fig. 5A).

Ammonium to DO ratios also aligned with the measurements of Fuchsman et al. (2015) and Hartnett and Devol (2003) at depths between 40 and 150 m but were smaller in magnitude than those of Berelson et al. (2013) which were measured at highly bioirrigated sites between 100 and 200 m near the Umpqua River depocenter (Fig. 5D). Phosphate to DO ratios showed similar values and variability to those of Berelson et al. (2013), generally falling into the same range of observed ratios between 0 to −0.04. For the OW-MS incubations, ratios of DIC to DO were mostly similar to those found by Berelson et al. (2013) during September off Oregon (Fig. 5C), and on the Northern California continental shelf. Silicate to DO ratios showed a larger range of variability

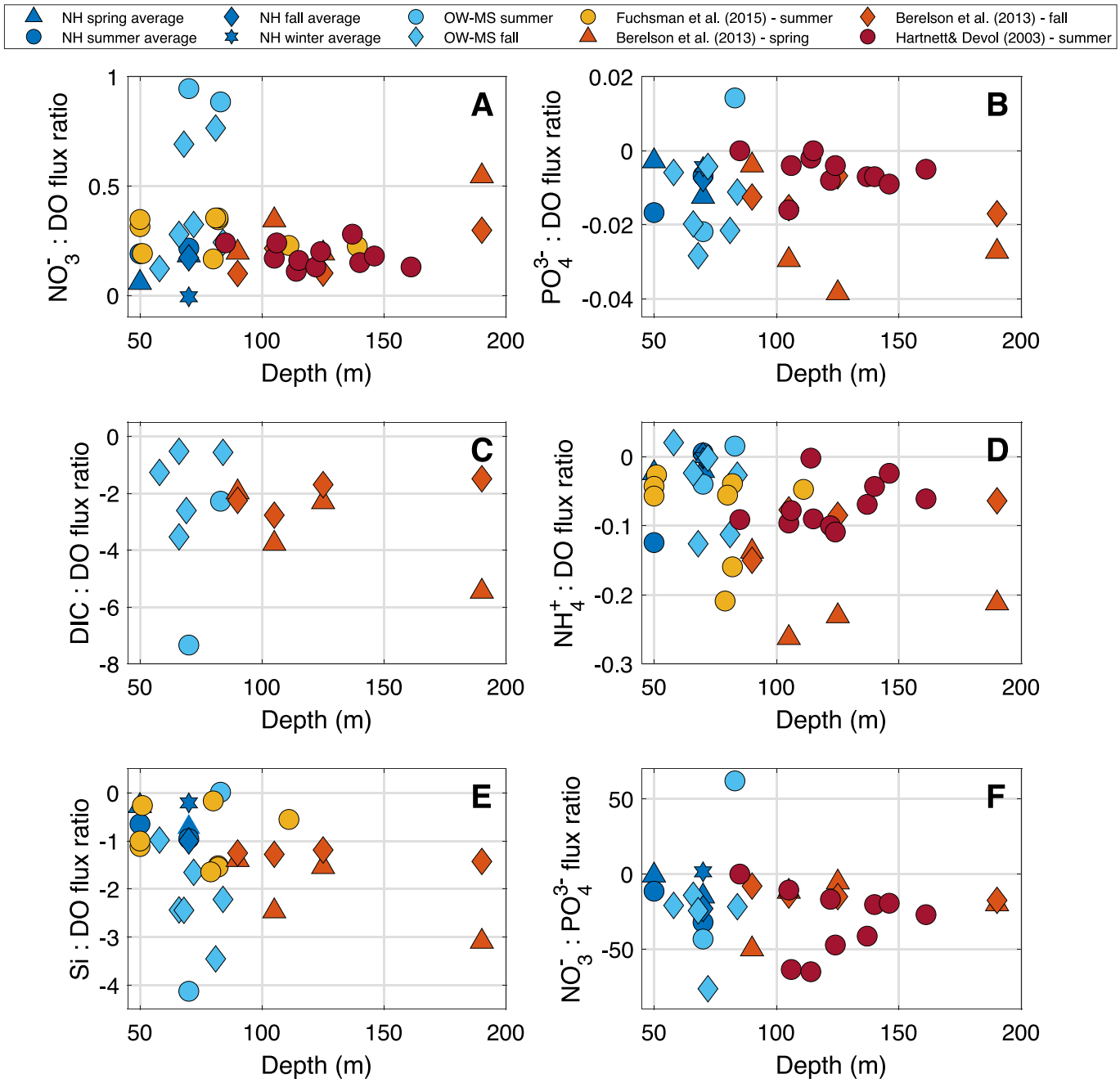

Fig. 5. Benthic flux ratios of NO_3^- (A), PO_4^{3-} (B), DIC (C), NH_4^+ (D), and Si (E) to DO, and NO_3^- to PO_4^{3-} (F), *versus* water depth for this study and previous studies on the Oregon-Washington shelf, with the studies differentiated by color and season of collection differentiated by marker shape.

amongst present and past studies compared with other flux ratios (Fig. 5E), with the ratios from the OW-MS 2022 dataset being relatively more negative compared with those of Berelson et al. (2013) and Fuchsman et al. (2015) at similar depths.

Overall, the flux ratios measured in this study with sediment core incubations, compared well to respective benthic flux ratios determined by *in situ* chambers especially when flux seasonality is taken into consideration. This suggests both approaches capture the same underlying sedimentary reactions.

4.2. Spatial and seasonal benthic flux variability

Factors most-likely to affect the incubation fluxes are the initial bottom water concentrations of chemical species and the availability of reactive carbon in surface sediments (Aller, 2014). Core incubation DO fluxes were between 1.5 and 2 times larger at the shallower, NH30 site compared with DO fluxes observed from the NH80 site, during similar times of the year (Fig. 2B, E, F and Fig. S6), analogous to DO flux differences at 30 m and 80 m observed in higher magnitude eddy covariance-based oxygen fluxes measured by McCann-Grosvenor et al. (2014) and Reimers and Fogaren (2021). Bottom water POC measurements showed higher amounts of POC in the benthic boundary layer at the NH30 site compared with the NH80 site throughout the year (Table S4). Benthic DO fluxes are generally found to decrease with increasing distance from coasts, due to both the tendency for planktonic biomass to be concentrated near the coast, resulting in larger particles that sink faster nearshore; and increasing water depth, resulting in a larger settling distance and longer oxygen exposure time for particles

before reaching sediments at greater depth (McCann-Grosvenor et al., 2014; Siedlecki et al., 2015). Nitrate and silicate fluxes showed strong seasonality but were generally similar in magnitude between the NH30 and NH80 sites, while ammonium fluxes appeared similar between NH30 and NH80 in the spring but were larger at NH30 in the summer (Table S3). These ammonium fluxes were inferred to be driven primarily by anaerobic respiration rates in subsurface layers of the sediment column.

In contrast to DO, nitrate, and silicate fluxes, phosphate fluxes did not exhibit a strict seasonal pattern (Fig. 2C, D, F and Fig. S6). Phosphate cycling in marine shelf sediments can be influenced by many factors including co-precipitation with iron oxyhydroxides and pulses of phytoplankton detritus (Berelson et al., 2003; Sundby et al., 1992). For example, using *ex situ* cores, Nixon (1981) measured an increase in phosphate fluxes from before to after the spring bloom in Narragansett Bay. In this study, phosphate fluxes were relatively low and out of the sediment during the late fall and winter and reached their peak during the summer at NH80 and early fall at the OW-MS sites, indicating higher rates of organic matter remineralization during this time (Fig. 2C and F). Higher ratios of phosphate to nitrate observed were also consistent with an increase in the contribution of denitrification and other anaerobic remineralization reactions within the sediment (Fig. 2C and F). However, some late spring and summer phosphate fluxes were into the sediment, which could be the result of phosphate binding to iron oxides present in surface sediment. Such inorganic reactions are also potentially important for reducing the benthic influence on water-column phosphate (Table 4) (Burdige, 2006).

4.3. Comparison of benthic flux exchange and bottom water property-property ratios

Under the assumption that organic matter, exported out of the surface layer, has a composition defined by classic Redfield ratios, the expected regeneration ratios of C:N:P can be prescribed, with deviations from these expected ratios informing remineralization pathways in the water column and in sediments. These regeneration ratios were computed for benthic fluxes, as the ratios of measured fluxes, and for bottom water data, as the property-property slopes of linear regressions, to assess the relationship between sediment and bottom water remineralization reactions, and how pathways may differ between these environments, across seasons, and at different sites on the OR-WA shelf. For bottom waters specifically, it is evident that aerobic remineralization is the dominant process controlling the property-property nutrient, DIC, and DO concentration relationships, as evidenced by the linear trends observed across all bottom water data at both NH30 and NH80 (Fig. 3), while for sediments, flux ratios show a much greater spread across sites and seasons (Fig. 2). Both bottom water and benthic flux ratios show seasonal variations at the NH line sites.

Winter benthic flux and bottom water chemistry ratios are consistent with decreased overall impacts of remineralization relative to mixing and of remineralization dominated by aerobic respiration, with low benthic phosphate fluxes, and benthic nitrate fluxes near zero (Fig. 2C), resulting in low ratios of nitrate to DO and nitrate to phosphate, which, along with benthic flux ratios of phosphate to DO, congregate close to the expected regeneration ratio for aerobic remineralization (Fig. 2C, E, F). Conversely at both the NH line and OW-MS sites, increased benthic flux exchange ratios of phosphate to DO and decreased ratios of nitrate to phosphate and DO were observed for the late spring, summer, and early fall, which are consistent with greater phosphate effluxes from and nitrate uptake by sediments during the upwelling season.

When bottom water oxygen concentrations are at their lowest, there is evidence that DIC concentrations may increase as a consequence of anaerobic organic matter oxidation (Fig. 3B). Anaerobic respiration in OR-WA margin sediments includes denitrification but also pathways of metal and sulfate reduction coupled to organic matter oxidation (Hartnett and Devol, 2003; Reimers et al., 2016). At the OW-MS sites anaerobic respiration is further indicated by respective phosphate and ammonium fluxes, similar to the flux values found by Berelson et al. (2013) along the Oregon-California margin. However, DIC additions could also be a byproduct of carbonate dissolution at the sediment-water interface as nearly all aragonite saturation states from bottom water collected at the OW-MS sites were less than 0.8 (Table S4).

4.4. Comparative estimates of benthic-pelagic coupling on the OR-WA shelf

The assessment of nutrient contributions from sediment fluxes in waters upwelled to the surface mixed layer, as measured by BEUTI indices, gave substantial spring and summer average percentage contributions for silicate but relatively low benthic contributions for phosphate (Table 4). These estimates while very rough are likely underestimates of the true benthic contribution due to their basis on NH line core incubations (rather than less available benthic chamber assessments) and the fact that the benthic fluxes of phosphate and silicate, measured at the additional OW-MS sites along the OR-WA shelf in the summer and early fall of 2022, were generally larger than those measured at NH line sites (Table S3). Additionally, although winter and fall values were excluded from this analysis, as downwelling conditions generally prevail during the winter, the surface mixed layer in winter can occasionally deepen to meet the bottom across the inner and mid-shelf regions (Perlin and Moum, 2008). Since both phosphate and silicate fluxes remain, generally, out of the sediment year-round (Table S3), during the late fall and winter, without the presence of prevailing upwelling but with an increase in the surface mixed layer and turbulence within the water column due to winter storms, the benthic contribution of phosphate and silicate to the water column is likely a key source of these major nutrients for winter surface water primary production.

4.5. Bottom water DO and N loss associated with sedimentary uptake

The eOMPA water mass analysis independently identified additional, year-round sinks for nitrate and DO in this region unaccounted for by water mass mixing or aerobic remineralization. For DO, these residuals are quite small (Fig. 4A) with respect to the observed DO concentration in bottom waters, likely a caveat of the eOMPA's limited capability to distinguish between DO uptake during aerobic remineralization in the water column compared with sediments. However, DO residuals from the eOMPA analysis were mostly positive year-round, signaling the water column impacts of a benthic sink. The DO residuals also appeared largest during the spring and at their lowest during the winter and late fall, which implies winter mixing and ventilation counteracts the higher benthic DO fluxes observed along the Oregon shelf during the winter (Reimers and Fogaren, 2021). Previous studies have estimated that respiration in sediments and the water column each contribute about 50 % (Connolly et al., 2010; Fuchsman et al., 2015) to DO losses from bottom waters on the OR-WA shelf, with areas of higher benthic contributions along the Washington shelf and at shallower, inner-shelf locations (Connolly et al., 2010). Further, some studies highlight the importance of bottom topography and retentive features, such as Heceta Bank on the Oregon shelf, in affecting these components and their variability, as such features can increase water mass residence time, enhancing DO draw down by both sediments and water-column remineralization (Adams et al., 2013; Fuchsman et al., 2015; Siedlecki et al., 2015).

The nitrate eOMPA residuals, in comparison to the magnitude of the DO residuals, are quite significant (Fig. 4B), and are also indicative of sediments acting as a net sink for fixed nitrogen. The nitrate residuals appeared largest during the summer and early fall and at their lowest during winter, which aligns well with both the pattern observed in nitrate fluxes at NH80 and the bottom water nitrate loss quantified using the NO tracer. Further, nitrate eOMPA residuals and N loss estimates quantified with the NO tracer were very similar in both seasonal

variability and magnitude (Table 3).

Using estimates of N_2 fluxes, calculated for underlying reaction balances (section 2.4), and estimates of bottom water N loss, calculated with the NO tracer (section 2.6), a simple model (Eq. 12) was applied to assess the processes contributing to observed bottom water N loss. This model revealed that bottom water N loss could readily be accounted for by sediment denitrification in the spring and summer, while calculations parameterized by early fall rates at the OW-MS sites indicated that it was less likely that benthic fluxes accounted for 100 % of the N loss on the shelf (Table 3). Thus, this result implies the possible presence of an additional bottom water N sink such as within water-column denitrification and consistent with findings of Segura-Noguera et al. (2023). These results indicate the need to better constrain the relative contributions of sediment and the water-column denitrification to fixed N deficits, and hold additional, significant implications for N limited primary productivity in this region (Bianchi et al., 2018; Fuchsman et al., 2015). Further, as noted by Bianchi et al. (2018), the sensitivity of water-column denitrification, associated with bound particles, to projected decreases in ocean DO is complicated, and requires additional direct observations to improve future modeling efforts.

For future studies it would be ideal to simultaneously constrain N_2 flux rates, BBL heights, water-column respiration rates, and transport on the OR-WA shelf more broadly to improve upon these assessments of sediment and water-column contributions to N and DO loss from bottom waters, particularly focusing on how these dynamics vary seasonally and interannually. Given the downward trend in DO content of upwelled source waters (Whitney et al., 2007) and the coupled nature of bottom water fixed N and oxygen availability, continuing to document the complex interplay between benthic remineralization and bottom water biogeochemistry, specifically in the context of seasonal upwelling dynamics, has major implications for understanding how this region may respond to future climate forcing.

5. Summary and conclusions

Paired sediment incubation flux and bottom water concentration data demonstrate the coupling between sediment and water-column remineralization processes and the variability resulting from water mass mixing and remineralization across the OR-WA shelf and across seasons at inner- and mid-shelf sites on the Oregon margin.

- *Ex situ* sediment incubation-based fluxes showed lower magnitudes, by a factor of between 1.5 and 3 on average, in comparison to past benthic flux studies, which had been determined with *in situ* benthic chamber incubations, for all measured parameters. When incubation fluxes were normalized to the respective DO flux, flux ratios from this study compared similarly to those from past *in situ* incubation studies of Fuchsman et al. (2015), Berelson et al. (2013), and Hartnett and Devol (2003), particularly for nitrate, phosphate, DIC, and ammonium, indicating that the measured flux ratios of this study represent relative rates of uptake and regeneration of these species within sediments.
- Benthic flux ratios of DO, nitrate, and phosphate showed seasonal variability along the NH line, with higher ratios of phosphate and nitrate to DO during the summer and fall and lower ratios during the winter. For the OW-MS sites, during the summer and early fall, benthic flux ratios amongst DO, nitrate, phosphate, and DIC indicated products released from anaerobic remineralization processes in support of previous findings in the region. Spatial variability in sediment remineralization patterns amongst OW-MS sites was also related to varying bottom water DO concentrations which during sampling in July and September 2022 ranged between 17 μmol kg^{-1} and 90 μmol kg^{-1}.
- A water mass analysis confirmed the importance of the sediments as a sink for DO and fixed inorganic nitrogen, particularly demonstrating a strengthened bottom water fixed N loss during the late summer and early fall.
- BEUTI indices enabled minimum, novel estimates of the percent contribution of benthic phosphate and silicate to upwelled waters, indicating sediments contribute on average 5 % and 37 % of respective upwelled phosphate and silicate, during the summer, and 2 % and 35 % of respective upwelled phosphate and silicate, during the spring. Phosphate and silicate returned from sediments to water-column inventories during periods when upwelling does not dominate are likely more critical for coupled primary production.
- A simple model was applied to estimates of N_2 fluxes and bottom water N loss, to constrain the benthic contribution to bottom water fixed N loss. Results showed that during the summer, N loss is reasonably 100 % attributable to sedimentary sinks. However, at a few sites with severely low DO conditions sampled in early fall, the presence of an additional fixed N sink, such as water-column denitrification appeared possible. These results are in support of previous findings by Segura-Noguera et al. (2023) and hold important implications for local primary productivity, which has been shown to be N-limited in the region.

Accurate spatiotemporal data to force and initialize benthic-pelagic coupling models is severely lacking (Ehrnsten et al., 2019). Further, the OR-WA shelf environment is a difficult environment to model benthic-pelagic coupling due to its dynamic nature, and high seasonal and interannual variability. These data provide cohesive, paired benthic flux and bottom water data, at the seasonal and spatial resolution required to improve model parameterization and validation.

The role of benthic-pelagic coupling on the OR-WA margin may be hypothesized to change under future climate scenarios. Future work should include more paired benthic flux and bottom water measurements at sites along the margin to broaden the spatial range, including more frequent outer shelf sampling and *in situ* benthic flux measurement methods such as chambers and eddy covariance as well. Future work may also include a deeper exploration of the influence of environmental factors on benthic flux variability. More specifically, the addition of relevant BBL height, residence time, and water-column remineralization rate measurements is needed to improve the accuracy and interpretation of the fixed N and DO uptake models applied in this study. Assessments of seasonal rates of bioirrigation and bioturbation would add insight to factors controlling benthic fluxes, and additional winter and fall measurements would enable an improved understanding of benthic-pelagic coupling during times of the year lacking in observations along the OR-WA margin.

Additionally, the development of the eOMPA model to include benthic aerobic and anaerobic remineralization components, using ratios determined from the incubations, would improve the ability of the eOMPA to quantify the benthic signal in bottom waters. This enhancement would expand the model's ability to capture benthic remineralization, in addition to water-column mixing and water-column remineralization, improving the model's ability to characterize benthic-pelagic coupling as a whole and to compare continental margins more broadly.

CRediT authorship contribution statement

Anna Hughes: Writing – review & editing, Writing – original draft, Validation, Software, Methodology, Investigation, Formal analysis, Data curation. **Clare E. Reimers:** Writing – review & editing, Validation, Supervision, Resources, Methodology, Investigation, Funding acquisition, Data curation, Conceptualization. **Kristen E. Fogaren:** Writing – review & editing, Validation, Methodology, Investigation, Data curation, Conceptualization. **Yvan Alleau:** Validation, Methodology, Investigation, Data curation, Conceptualization.

Declaration of competing interest

None.

Acknowledgements

This work was supported by grants from the National Science Foundation to C. Reimers [grant numbers OCE-1634319, OCE-2126112, OCE-1748726]. We are grateful to the crews, marine technicians, and research assistants aboard the R/*Vs Oceanus* and *Robert Gordon Sproul* for their contributions to at sea operations and sampling, especially Marnie Jo Zirbel and Abby Tomita who assisted with the sediment incubation experiments. We would like to thank J. Jennings and D. Hubbard for executing the nutrient analyses, as well as two anonymous reviewers for their constructive and insightful comments which greatly improved this manuscript.

Appendix A. Supplementary data

Supplementary data to this article can be found online at https://doi.org/10.1016/j.marchem.2024.104473.

Data availability

All bottom water data are available at 10.26008/1912/bco-dmo.793115.1 for all NH line cruises in 2017–2019 and at 10.26008/1912/bco-dmo.880760.1 for the OW-MS cruises in 2022. All benthic flux data is available at 10.26008/1912/bco-dmo.940414.1.

References

Adams, K.A., Barth, J.A., Chan, F., 2013. Temporal variability of near-bottom dissolved oxygen during upwelling off Central Oregon. J. Geophys. Res. Oceans 118 (10), 4839–4854.
Aller, R.C., 2014. 8.11 - sedimentary diagenesis, depositional environments, and benthic fluxes. In: Holland, H.D., Turekian, K.K. (Eds.), Treatise on Geochemistry (Second Edition). Elsevier, Oxford, pp. 293–334.
Aller, R., Aller, J., 1998. The effect of biogenic irrigation intensity and solute exchange on diagenetic reaction rates in marine sediments. J. Mar. Res. 56, 905–936.
Aller, R.C., Rude, P.D., 1988. Complete oxidation of solid phase sulfides by manganese and bacteria in anoxic marine sediments. Geochim. Cosmochim. Acta 52 (3), 751–765.
Alonso-Pérez, F., Castro, C., 2014. Benthic oxygen and nutrient fluxes in a coastal upwelling system (ria de Vigo, NW Iberian Peninsula): seasonal trends and regulating factors. Mar. Ecol. Prog. Ser. 511, 17–32.
Anderson, L.A., Sarmiento, J.L., 1994. Redfield ratios of remineralization determined by nutrient data analysis. Glob. Biogeochem. Cycles 8 (1), 65–80.
Archer, D., Devol, A., 1992. Benthic oxygen fluxes on the Washington shelf and slope: a comparison of in situ microelectrode and chamber flux measurements. Limnol. Oceanogr. 37 (3), 614–629.
Barth, J.A., Wheeler, P.A., 2005. Introduction to special section: coastal advances in shelf transport. J. Geophys. Res. Oceans 110 (C10).
Barth, J.A., Pierce, S.D., Castelao, R.M., 2005. Time-dependent, wind-driven flow over a shallow midshelf submarine bank. J. Geophys. Res. Oceans 110 (C10).
Bauer, J.E., Cai, W.-J., Raymond, P.A., Bianchi, T.S., Hopkinson, C.S., Regnier, P.A.G., 2013. The changing carbon cycle of the coastal ocean. Nature 504 (7478), 61–70.
Berelson, W., McManus, J., Coale, K., Johnson, K., Burdige, D., Kilgore, T., Colodner, D., Chavez, F., Kudela, R., Boucher, J., 2003. A time series of benthic flux measurements from Monterey Bay, CA. Cont. Shelf Res. 23 (5), 457–481.
Berelson, W.M., McManus, J., Severmann, S., Reimers, C.E., 2013. Benthic flux of oxygen and nutrients across Oregon/California shelf sediments. Cont. Shelf Res. 55, 66–75.
Berg, P., Hans, R.Â.Y., Felix, J., Volker, M., Bo Barker, J.Â.R., Markus, H., de Dirk, B., 2003. Oxygen uptake by aquatic sediments measured with a novel non-invasive eddy-correlation technique. Mar. Ecol. Prog. Ser. 261, 75–83.
Berg, P., Røy, H., Wiberg, P.L., 2007. Eddy correlation flux measurements: the sediment surface area that contributes to the flux. Limnol. Oceanogr. 52 (4), 1672–1684.
Berg, P., Huettel, M., Glud, R.N., Reimers, C.E., Attard, K.M., 2022. Aquatic eddy covariance: the method and its contributions to defining oxygen and carbon fluxes in marine environments. Annu. Rev. Mar. Sci. 14 (1), 431–455.
Bianchi, D., Weber, T.S., Kiko, R., Deutsch, C., 2018. Global niche of marine anaerobic metabolisms expanded by particle microenvironments. Nat. Geosci. 11 (4), 263–268.
Blackburn, T., Henriksen, K., 1983. Nitrogen cycling in different types of sediments from Danish waters 1. Limnol. Oceanogr. 28 (3), 477–493.
Bograd, S.J., Castro, C.G., Di Lorenzo, E., Palacios, D.M., Bailey, H., Gilly, W., Chavez, F. P., 2008. Oxygen declines and the shoaling of the hypoxic boundary in the California current. Geophys. Res. Lett. 35 (12).
Broecker, W.S., 1974. "NO", a conservative water-mass tracer. Earth Planet. Sci. Lett. 23 (1), 100–107.
Burdige, D.J., 2006. Geochemistry of Marine Sediments. Princeton University Press.
Caffrey, J.M., Hollibaugh, J.T., Bano, N., Haskins, J., 2010. Effects of upwelling on short-term variability in microbial and biogeochemical processes in estuarine sediments from Elkhorn Slough, California, USA. Aquat. Microb. Ecol. 58 (3), 261–271.
Canfield, D.E., 1994. Factors influencing organic carbon preservation in marine sediments. Chem. Geol. 114 (3), 315–329.
Chan, F., Barth, J., Lubchenco, J., Kirincich, A., Weeks, H., Peterson, W.T., Menge, B., 2008. Emergence of anoxia in the California current large marine ecosystem. Science 319 (5865), 920.
Chase, Z., van Geen, A., Kosro, P.M., Marra, J., Wheeler, P.A., 2002. Iron, nutrient, and phytoplankton distributions in Oregon coastal waters. J. Geophys. Res. Oceans 107 (C10), 38-1-38-17.
Chase, Z., Hales, B., Cowles, T., Schwartz, R., van Geen, A., 2005. Distribution and variability of iron input to Oregon coastal waters during the upwelling season. J. Geophys. Res. Oceans 110 (C10).
Chavez, F.P., Pennington, J.T., Michisaki, R.P., Blum, M., Chavez, G.M., Friederich, J., Jones, B., Herlien, R., Kieft, B., Hobson, B., 2017. Climate variability and change: response of a coastal ocean ecosystem. Oceanography 30 (4), 128–145.
Codispoti, L.A., 2007. An oceanic fixed nitrogen sink exceeding 400 Tg N a-1 vs the concept of homeostasis in the fixed-nitrogen inventory. Biogeosciences 4 (2), 233–253.
Connolly, T.P., Hickey, B.M., Geier, S.L., Cochlan, W.P., 2010. Processes influencing seasonal hypoxia in the northern California current system. J. Geophys. Res. Oceans 115 (C3).
Cowan, J.L., Pennock, J.R., Boynton, W.R., 1996. Seasonal and interannual patterns of sediment-water nutrient and oxygen fluxes in Mobile Bay, Alabama (USA): regulating factors and ecological significance. Mar. Ecol. Prog. Ser. 141, 229–245.
Culberson, C.H., Knapp, G.P., Stalcup, M.C., Williams, R.T., Zemlyak, F., 1991. A Comparison of Methods for the Determination of Dissolved Oxygen in Seawater.
Dale, A.W., Graco, M., Wallmann, K., 2017. Strong and dynamic benthic-pelagic coupling and feedbacks in a coastal upwelling system (Peruvian shelf). Front. Mar. Sci. 4.
Deutsch, C., Frenzel, H., McWilliams, J.C., Renault, L., Kessouri, F., Howard, E., Liang, J.-H., Bianchi, D., Yang, S., 2021. Biogeochemical variability in the California current system. Prog. Oceanogr. 196, 102565.
Devol, A.H., Christensen, J.P., 1993. Benthic fluxes and nitrogen cycling in sediments of the continental margin of the eastern North Pacific. J. Mar. Res. 51 (2), 345–372.
Ehrnsten, E., Norkko, A., Timmermann, K., Gustafsson, B.G., 2019. Benthic-pelagic coupling in coastal seas–modelling macrofaunal biomass and carbon processing in response to organic matter supply. J. Mar. Syst. 196, 36–47.
Evans, W., Pocock, K., Hare, A., Weekes, C., Hales, B., Jackson, J., Gurney-Smith, H., Mathis, J.T., Alin, S.R., Feely, R.A., 2019. Marine CO2 patterns in the northern Salish Sea. Front. Mar. Sci. 5, 536.
Fleischbein, J., 2001. CTD data from 37 cruises of the California Current System (CCS) Long-Term Observation Program (LTOP) in the Northeast Pacific from 1997-2004 as part of the U.S. GLOBEC Program (NEP project). Biological and Chemical Oceanography Data Management Office (BCO-DMO).
Fuchsman, C.A., Devol, A.H., Chase, Z., Reimers, C.E., Hales, B., 2015. Benthic fluxes on the Oregon shelf. Estuar. Coast. Shelf Sci. 163, 156–166.
Galán, A., Zirbel, M.J., Saldías, G.S., Chan, F., Letelier, R., 2020. The role of upwelling intermittence in the development of hypoxia and nitrogen loss over the Oregon shelf. J. Mar. Syst. 207, 103342.
Gattuso, J.-P., Frankignoulle, M., Wollast, R., 1998. Carbon and carbonate metabolism in coastal aquatic ecosystems. Annu. Rev. Ecol. Syst. 29 (1), 405–434.
Glud, R.N., 2008. Oxygen dynamics of marine sediments. Mar. Biol. Res. 4 (4), 243–289.
Glud, R., Blackburn, N., 2002. The effects of chamber size on benthic oxygen uptake measurements: a simulation study. Ophelia 56 (1), 23–31.
Glud, R.N., Gundersen, J.K., Jørgensen, B.B., Revsbech, N.P., Schulz, H.D., 1994. Diffusive and total oxygen uptake of deep-sea sediments in the eastern South Atlantic Ocean: in situ and laboratory measurements. Deep-Sea Res. I Oceanogr. Res. Pap. 41 (11–12), 1767–1788.
Glud, R.N., Holby, O., Hoffmann, F., Canfield, D.E., 1998. Benthic mineralization and exchange in Arctic sediments (Svalbard, Norway). Mar. Ecol. Prog. Ser. 173, 237–251.
Glud, R.N., Gundersen, J.K., Røy, H., Jørgensen, B.B., 2003. Seasonal dynamics of benthic O_2 uptake in a semienclosed bay: importance of diffusion and faunal activity. Limnol. Oceanogr. 48 (3), 1265–1276.
Goñi, M.A., Welch, K.A., Alegria, E., Alleau, Y., Watkins-Brandt, K., White, A.E., 2021. Wintertime particulate organic matter distributions in surface waters of the northern California current system. Cont. Shelf Res. 213, 104312.
Gordon, L.I., Jennings Jr., J.C., Ross, A.A., Krest, J.M., 1993. A suggested protocol for continuous flow automated analysis of seawater nutrients (phosphate, nitrate, nitrite and silicic acid) in the WOCE hydrographic program and the joint Global Ocean fluxes study. In: WOCE Hydrographic Program Office, Methods Manual WHPO(68/91), pp. 1–52.
Grenz, C., Cloern, J.E., Hager, S.W., Cole, B.E., 2000. Dynamics of nutrient cycling and related benthic nutrient and oxygen fluxes during a spring phytoplankton bloom in South San Francisco Bay (USA). Mar. Ecol. Prog. Ser. 197, 67–80.
Grenz, C., Denis, L., Pringault, O., Fichez, R., 2010. Spatial and seasonal variability of sediment oxygen consumption and nutrient fluxes at the sediment water interface in a sub-tropical lagoon (New Caledonia). Mar. Pollut. Bull. 61 (7–12), 399–412.

Griffiths, J.R., Kadin, M., Nascimento, F.J.A., Tamelander, T., Törnroos, A., Bonaglia, S., Bonsdorff, E., Brüchert, V., Gårdmark, A., Järnström, M., Kotta, J., Lindegren, M., Nordström, M.C., Norkko, A., Olsson, J., Weigel, B., Žydelis, R., Blenckner, T., Niiranen, S., Winder, M., 2017. The importance of benthic–pelagic coupling for marine ecosystem functioning in a changing world. Glob. Chang. Biol. 23 (6), 2179–2196.
Hales, B., Chipman, D., Takahashi, T., 2004. High-frequency measurement of partial pressure and total concentration of carbon dioxide in seawater using microporous hydrophobic membrane contactors. Limnol. Oceanogr. Methods 2 (11), 356–364.
Hales, B., Karp-Boss, L., Perlin, A., Wheeler, P.A., 2006. Oxygen production and carbon sequestration in an upwelling coastal margin. Glob. Biogeochem. Cycles 20 (3).
Hartnett, H.E., Devol, A.H., 2003. Role of a strong oxygen-deficient zone in the preservation and degradation of organic matter: a carbon budget for the continental margins of Northwest Mexico and Washington state. Geochim. Cosmochim. Acta 67 (2), 247–264.
Hickey, B.M., 1979. The California current system—hypotheses and facts. Prog. Oceanogr. 8 (4), 191–279.
Hickey, B.M., Banas, N.S., 2003. Oceanography of the US Pacific northwest coastal ocean and estuaries with application to coastal ecology. Estuaries 26, 1010–1031.
Hughes, A.R., 2024. Spatiotemporal Variability in Benthic-Pelagic Coupling on the Oregon-Washington Shelf: An Investigation of Bottom Water and Benthic Flux Data. Masters Thesis,. Oregon State University.
Huyer, A., 1977. Seasonal variation in temperature, salinity, and density over the continental shelf off Oregon 1. Limnol. Oceanogr. 22 (3), 442–453.
Huyer, A., 1983. Coastal upwelling in the California current system. Prog. Oceanogr. 12 (3), 259–284.
Huyer, A., Sobey, E., Smith, R.L., 1979. The spring transition in currents over the Oregon continental shelf. J. Geophys. Res. Oceans 84 (C11), 6995–7011.
Huyer, A., Wheeler, P.A., Strub, P.T., Smith, R.L., Letelier, R., Kosro, P.M., 2007. The Newport line off Oregon–Studies in the north east Pacific. Prog. Oceanogr. 75 (2), 126–160.
Jacox, M.G., Edwards, C.A., Hazen, E.L., Bograd, S.J., 2018. Coastal upwelling revisited: Ekman, Bakun, and improved upwelling indices for the US west coast. J. Geophys. Res. Oceans 123 (10), 7332–7350.
Jahnke, R.A., 1996. The global ocean flux of particulate organic carbon: areal distribution and magnitude. Glob. Biogeochem. Cycles 10 (1), 71–88.
Jørgensen, B.B., Wenzhöfer, F., Egger, M., Glud, R.N., 2022. Sediment oxygen consumption: role in the global marine carbon cycle. Earth Sci. Rev. 228, 103987.
Kalvelage, T., Jensen, M.M., Contreras, S., Revsbech, N.P., Lam, P., Günter, M., Laroche, J., Lavik, G., Kuypers, M.M.M., 2011. Oxygen sensitivity of Anammox and coupled N-cycle processes in oxygen minimum zones. PLoS One 6 (12), e29299.
Kelly, J.R., Nixon, S.W., 1984. Experimental studies of the effect of organic deposition on the metabolism of a coastal marine bottom community. Marine Ecolo. Progr. Seri. Oldendorf 17 (2), 157–169.
Kniskern, T.A., Warrick, J., Farnsworth, K.L., Wheatcroft, R.A., Goni, M.A., 2011. Coherence of river and ocean conditions along the US west coast during storms. Cont. Shelf Res. 31 (7–8), 789–805.
Kopp, D., Lefebvre, S., Cachera, M., Villanueva, M.C., Ernande, B., 2015. Reorganization of a marine trophic network along an inshore–offshore gradient due to stronger pelagic–benthic coupling in coastal areas. Prog. Oceanogr. 130, 157–171.
Kriest, I., Oschlies, A., 2008. On the treatment of particulate organic matter sinking in large-scale models of marine biogeochemical cycles. Biogeosciences 5 (1), 55–72.
Kurapov, A.L., Allen, J.S., Egbert, G.D., Miller, R.N., Kurapov, A.L., Allen, J.S., Egbert, G. D., Miller, R.N., 2005. Modeling bottom mixed layer variability on the mid-Oregon shelf during summer upwelling. J. Phys. Oceanogr. 35 (9).
Landry, M., Postel, J., Peterson, W., Newman, J., 1989. Broad-scale distributional patterns of hydrographic variables on the Washington/Oregon shelf. In: Elsevier Oceanography Series. Elsevier, pp. 1–40.
Mazzini, P.L., Barth, J.A., Shearman, R.K., Erofeev, A., 2014. Buoyancy-driven coastal currents off Oregon during fall and winter. J. Phys. Oceanogr. 44 (11), 2854–2876.
McCann-Grosvenor, K., Reimers, C.E., Sanders, R.D., 2014. Dynamics of the benthic boundary layer and seafloor contributions to oxygen depletion on the Oregon inner shelf. Cont. Shelf Res. 84, 93–106.
McDougall, T.J., Barker, P.M., 2011. Getting started with TEOS-10 and the Gibbs seawater (GSW) oceanographic toolbox. Scor/Iapso WG 127 (532), 1–28.
McManus, D.A., 1972. Bottom Topography and Sediment Texture near the Columbia River Mouth.
Middelburg, J.J., Vlug, T., Jaco, F., Van der Nat, W., 1993. Organic matter mineralization in marine systems. Glob. Planet. Chang. 8 (1–2), 47–58.
Millero, F.J., 2010. Carbonate constants for estuarine waters. Mar. Freshw. Res. 61 (2), 139–142.
Nittrouer, C., Sternberg, R., 1981. The formation of sedimentary strata in an allochthonous shelf environment: the Washington continental shelf. In: Developments in Sedimentology. Elsevier, pp. 201–232.
Nixon, S.W., 1981. Freshwater inputs and estuarine productivity. In: Proceedings of the National Symposium on Freshwater inflow to Estuaries. US Department of the Interior Washington, pp. 31–57.
Paulmier, A., Kriest, I., Oschlies, A., 2009. Stoichiometries of remineralisation and denitrification in global biogeochemical ocean models. Biogeosciences 6 (5), 923–935.
Perlin, A., Moum, J.N., 2008. Structure of Downwelling on the Oregon Continental Shelf, pp. OS41B-1224.
Perlin, A., Moum, J.N., Klymak, J.M., 2005. Response of the bottom boundary layer over a sloping shelf to variations in alongshore wind. J. Geophys. Res. Oceans 110 (C10).
Reimers, C.E., Fogaren, K.E., 2021. Bottom boundary layer oxygen fluxes during winter on the Oregon shelf. J. Geophys. Res. Oceans 126 (3), e2020JC016828.
Reimers, C.E., Özkan-Haller, H.T., Berg, P., Devol, A., McCann-Grosvenor, K., Sanders, R. D., 2012. Benthic oxygen consumption rates during hypoxic conditions on the Oregon continental shelf: evaluation of the eddy correlation method. J. Geophys. Res. Oceans 117 (C2).
Reimers, C.E., Özkan-Haller, H.T., Sanders, R.D., McCann-Grosvenor, K., Chace, P.J., Crowe, S.A., 2016. The dynamics of benthic respiration at a mid-shelf station off Oregon. Aquat. Geochem. 22, 505–527.
Rowe, G.T., Clifford, C.H., Smith, K.L., Hamilton, P.L., 1975. Benthic nutrient regeneration and its coupling to primary productivity in coastal waters. Nature 255, 5505, 255(5505).
Sarmiento, J.L., 2006. Ocean Biogeochemical Dynamics. Princeton University Press.
Segura-Noguera, M., Álvarez-Salgado, X.A., Siedlecki, S., Hales, B.R., 2023. Short time-scale variability of ammonium, nitrate, and nitrogen loss dynamics during an upwelling-induced bloom at the Oregon shelf. J. Geophys. Res. Oceans 128 (6), e2022JC019025.
Severmann, S., McManus, J., Berelson, W.M., Hammond, D.E., 2010. The continental shelf benthic iron flux and its isotope composition. Geochim. Cosmochim. Acta 74 (14), 3984–4004.
Sharp, J.D., Pierrot, D., Humphreys, M.P., Epitalon, J.-M., Orr, J.C., Lewis, E.R., Wallace, D.W.R., 2020. CO2SYSv3 for MATLAB (v3.0). Zenodo.
Shrikumar, A., Lawrence, R., Casciotti, K.L., 2022. PYOMPA Version 0.3: Technical Note. ESS Open Archive.
Siedlecki, S.A., Banas, N.S., Davis, K.A., Giddings, S., Hickey, B.M., MacCready, P., Connolly, T., Geier, S., 2015. Seasonal and interannual oxygen variability on the Washington and Oregon continental shelves. J. Geophys. Res. Oceans 120 (2), 608–633.
Sundby, B., Gobeil, C., Silverberg, N., Alfonso, M., 1992. The phosphorus cycle in coastal marine sediments. Limnol. Oceanogr. 37 (6), 1129–1145.
Thunell, R., Benitez-Nelson, C., Varela, R., Astor, Y., Muller-Karger, F., 2007. Particulate organic carbon fluxes along upwelling-dominated continental margins: rates and mechanisms. Glob. Biogeochem. Cycles 21 (1).
Tomczak, M., 1981. A multi-parameter extension of temperature/salinity diagram techniques for the analysis of non-isopycnal mixing. Prog. Oceanogr. 10 (3), 147–171.
Tomczak, M., 1999. Some historical, theoretical and applied aspects of quantitative water mass analysis. J. Mar. Res. 57, 275–303.
Torres, M.E., Mix, A.C., Rugh, W.D., 2005. Precise δ13C analysis of dissolved inorganic carbon in natural waters using automated headspace sampling and continuous-flow mass spectrometry. Limnol. Oceanogr. Methods 3 (8), 349–360.
Trimmer, M., Nedwell, D., Sivyer, D., Malcolm, S., 1998. Nitrogen fluxes through the lower estuary of the river great Ouse, England: the role of the bottom sediments. Mar. Ecol. Prog. Ser. 163, 109–124.
van de Velde, S.J., Hylén, A., Eriksson, M., James, R.K., Kononets, M.Y., Robertson, E.K., Hall, P.O.J., 2023. Exceptionally high respiration rates in the reactive surface layer of sediments underlying oxygen-deficient bottom waters. Proceed. Royal Soc. A: Mathemat. Phys. Eng. Sci. 479 (2275), 20230189.
Varela, M., Prego, R., Pazos, Y., 2004. Vertical biogenic particle flux in a western Galician ria (NW Iberian Peninsula). Mar. Ecol. Prog. Ser. 269, 17–32.
Verardo, D.J., Froelich, P.N., McIntyre, A., 1990. Determination of organic carbon and nitrogen in marine sediments using the Carlo Erba NA-1500 analyzer. Deep Sea Re. Part A. Oceanogr. Res. Pape. 37 (1), 157–165.
Walsh, J.J., 1991. Importance of continental margins in the marine biogeochemical cycling of carbon and nitrogen. Nature 350 (6313), 53–55.
Whitney, F.A., Freeland, H.J., Robert, M., 2007. Persistently declining oxygen levels in the interior waters of the eastern subarctic Pacific. Prog. Oceanogr. 75 (2), 179–199.
Wyatt, A.M., Resplandy, L., Marchetti, A., 2022. Ecosystem impacts of marine heat waves in the Northeast Pacific. Biogeosciences 19 (24), 5689–5705.